ChemPhysChem

Research Article
doi.org/10.1002/cphc.202300114

Chemistry Europe
European Chemical Societies Publishing

www.chemphyschem.org

Is DFT Accurate Enough to Calculate Regioselectivity? The Case of 1,3-Dipolar Cycloaddition of Azide to Alkynes and Alkenes

Giorgio Molteni[a] and Alessandro Ponti*[b]

The importance of regioselectivity in 1,3-dipolar cycloadditions (DCs) makes it surprising that no benchmarking study on this problem has appeared. We investigated whether DFT calculations are an accurate tool to predict the regioselectivity of uncatalyzed thermal azide 1,3-DCs. We considered the reaction between HN_3 and 12 dipolarophiles, comprising ethynes HC≡C–R and ethenes H_2C=CH–R (R=F, OH, NH_2, Me, CN, CHO), which cover a broad range of electron demand and conjugation ability.

We established benchmark data by the W3X protocol [complete-basis-set-extrapolated CCSD(T)-F12 energy with T-(T) and (Q) corrections and MP2-calculated core/valence and relativistic effects] and showed that core/valence effects and high-order excitations are important for accurate regioselectivity.

Regioselectivities calculated using an extensive set of density functional approximations (DFAs) were compared with benchmark data. Range-separated and meta-GGA hybrids gave the best results. Good treatment of self-interaction and electron exchange are the key features for accurate regioselectivity. Dispersion correction slightly improves agreement with W3X results. The best DFAs provide the isomeric TS energy difference with an expected error ≈0.7 mh and errors ≈2 mh can occur. The isomer yield provided by the best DFA has an expected error of ±5%, though errors up to 20% are not rare. At present, an accuracy of 1–2% is unfeasible but it seems that we are not far from achieving this goal.

Introduction

Site-, regio- and stereoselectivity are issues that have received much attention in the practice of modern organic chemistry. Many challenges in relation to these three topics have been overcome, but much work remains to be done. Restricting ourselves to the field of 1,3-dipolar cycloaddition (1,3-DC) chemistry, the site selectivity of these processes is always dictated by the presence of an appropriate dipolarophilic function, invariably represented by an unsaturated site consisting of an identical or different pair of atoms. The huge field of stereoselective 1,3-DCs has been investigated extensively in the last three decades from both synthetic and theoretical perspectives.[1] The problem of regioselectivity in 1,3-DCs, however, concerns the very birth of this type of reaction. From both Huisgen's pioneering studies in the late 1950s on 1,3-DCs and those concerning the related Diels–Alder cycloadditions, an uncomfortable picture was drawn about the lack of rationalization of their regioselectivities. This situation was summarized with a hint of bitterness by Doering in the term "no mechanism reactions".[2] The picture of the regioselectivity of these concerted processes was destined to change radically after the enunciation of the Woodward-Hoffman rules,[3] which describe the regioselectivity of these concerted processes by binding it to the principle of conservation of symmetry of interacting orbitals.

A further step forward in the field of regioselectivity of 1–3DCs was taken with the advent and application of concepts related to frontier orbitals (FMOs), due to the studies by Fukui.[4,5] The energetically favorable interaction between the HOMO (or LUMO, in reverse demand cycloadditions) of the dipolar species and the LUMO (or HOMO) of the dipolarophilic species finally gave a sure indication of the regioselectivity of 1,3-DCs. This was the background to Houk's two masterful papers of 1973,[6,7] in which the regioselectivity of 1,3-DC was rationalized systematically for all 1,3-dipolar species using semiempirical methods. Unfortunately, there are many exceptions to the regioselectivity predicted through this approach. The discrepancies from the experimental data can be traced back to the perturbative nature of the approach and use of atomic orbital coefficients in FMOs calculated by heavily approximated methods. As an example, the regioselectivity of phenylazides with respect to methyl propiolate cannot be rationalized on the basis of the electronic demands of the reactants or FMO theory.[8] More recently, the Complete Basis

[a] Dr. G. Molteni
Dipartimento di Chimica
Università degli Studi di Milano
Via C. Golgi 19, 20133 Milano (Italy)
[b] Dr. A. Ponti
Istituto di Scienze e Tecnologie Chimiche "Giulio Natta"
Consiglio Nazionale delle Ricerche
Via C. Golgi 19, 20133 Milano (Italy)
E-mail: alessandro.ponti@scitec.cnr.it

Supporting information for this article is available on the WWW under https://doi.org/10.1002/cphc.202300114

Set-Quadratic Becke3 (CBS-QB3) protocol[9] was used to calculate the activation barrier of the 1,3-DC of the nine "canonical" dipoles to ethene or ethyne, and based on these data the "distortion/interaction principle" was proposed, according to which the 1,3-dipolar species first distorts to reach a reactive state, and the subsequent addition to the dipolarophile occurs with a barrier that does not depend on the exothermicity of the cycloaddition and on the FMO interactions.[10–12] Unfortunately, this brilliant theoretical approach does not constitute a general approach in the prediction of regioselectivity in 1,3-DCs, also because surprisingly large deviations for the CBS-QB3 protocol with respect to the more advanced W1-F12[13] and W2-F12[13] protocols have been found, raising some questions upon the suitability of CBS-QB3 as a reference protocol.[14]

In the last 30 years, Density Functional Theory (DFT) has become the most popular approach to molecular electronic structure calculations.[15,16] DFT has been applied to 1,3-DCs, but most reports focus on the activation barrier and regioselectivity is seldom treated.[17] Conceptual DFT[18] naturally focus on the regioselectivity problem,[19] which is investigated using Fukui and local softness functions, and a quantitative formulation of regioselectivity.[20,21] This approach has been applied to the azide 1,3-DC reaction.[8,22–25] Also the Molecular Electron Density Theory[26] has been applied to the regioselectivity of azide 1,3-DCs.[27,28]

Since DFT calculations are feasible for large systems, they have sometimes been used to calculate with reasonable accuracy the isomeric ratio of reactions of interest for the synthetic chemist. It was the case for cycloadditions between phenylazides and enamines[29] and between azides and strained (unsymmetrical) alkynes and alkenes.[30,31] Also within the framework of DFT theory, accurate predictions of regioselectivity in cycloaddition between phenylazides and propargyl alcohol,[32] methyl propiolate[8] and alkenes[25] have been possible. The Activation Strain Analysis approach has been used to understand the regioselectivity of the cycloaddition of HN_3 and MeN_3 to monosubstituted alkenes,[12] and between MeN_3 and linear and cyclic allenes,[33] highlighting the importance of the interaction term.

A huge number of approximations to the true density functional have been proposed[16] and the chemist has to choose the density functional approximation (DFA) best suited for the task at hand. Such decision is usually taken based on benchmarking studies, where DFAs are compared with experimental data or results from high-level, wavefunction-based protocols. The 1,3-DC of the nine "canonical" dipoles to ethene constitutes Set II of the BHPERI database (activation barriers of pericyclic reactions), which is part of the GMTKN55 database.[34] The ability of DFAs to reproduce the benchmark activation barriers of 1,3-DCs has been investigated more than once,[14,16,35] but we are not aware of similar studies focusing of the regioisomeric ratio of 1,3-DCs.

It may seem strange that many of the studies on the regioselectivity of 1,3-DCs involve azides. From a synthetic chemistry standpoint, this is justified because it is possible to obtain the 1,2,3-triazoles produced by metal-catalyzed cycloadditions as single regioisomers: 4-substituted isomers arise with Cu(I) catalysis,[36,37] and 5-substituted one are obtained in the presence of Ru(II),[38] Ni(II),[39] and Ir(II) catalysts.[40] Second, 1,2,3-triazoles have found a number of applications as pharmaceuticals since they may display a wide range of biological activities.[41] Furthermore, 1,2,3-triazoles have also found wide use in industrial applications as dyes, corrosion inhibition, photographic materials, and nitrification inhibitors.[42] From the theoretical standpoint, notwithstanding the activation barriers of 1,3-dipolar cycloadditions have been a favorite playground for computational chemists, we are not aware of systematic computational studies on the regioisomerism of 1,3-DCs.

For all these reasons, we decided to investigate whether DFT calculations can be established as an accurate tool to predict the regioselectivity output of uncatalyzed thermal azide 1,3-DCs, since these widely used reactions yield the two regioisomeric 1,2,3-triazoles when the dipolarophilic counterpart is asymmetric. We chose a set of the smallest systems giving rise to isomerism, i.e., we considered the reaction between the 1,3-dipole hydrazoic acid HN_3 (as a model for organic azides) and a set of 12 dipolarophiles, comprising the monosubstituted ethynes HC≡C–R and ethenes H_2C=CH–R (R=F, OH, NH_2, Me, CN, CHO) covering a broad range of electron demand and conjugation ability. Two regiosomeric products are possible: the 4-R- and 5-R-substituted 1,2,3-triazoles and 1,2,3-triazolines (Scheme 1). According to Houk's classification of substituted ethenes,[6] CHO and CN are conjugating, electron-withdrawing substituents (Z class); F, OH, and NH_2 are powerful electron-donors (X class) and Me is an alkyl weak donor (R class). The investigated substituent set thus covers all of Houk's classes, except for purely conjugating substituents (C class, for example, vinyl, phenyl). Although the considered dipolarophiles are generally stable molecules, in some cases they actually exist as minor tautomer of the corresponding "keto" form, for example, H_2C=CH–OH and HC≡C–OH are the minor tautomer, respectively, of acetaldehyde H_3C–CHO and ketene H_2C=C=O.

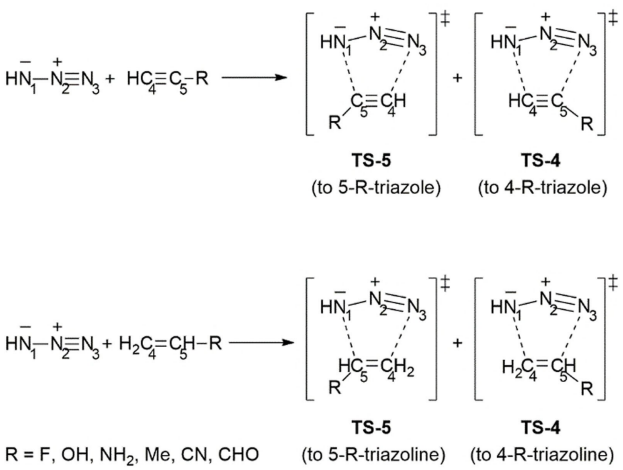

Scheme 1. Schematic depiction of the isomeric transition states of the 1,3-dipolar cycloadditions of HN_3 to HC≡C–R and H_2C=CH–R (R=F, OH, NH_2, Me, CN, CHO) yielding the 4-R- and 5-R-substituted 1,2,3-triazoles and 1,2,3-triazolines.

In the lack of high-quality gas-phase data for the above reactions, we used wavefunction-based computational protocols of the W*n* (*n* = 1, 2, 3) family[43] to calculate reference values for the regioselectivity of the considered 1,3-DCs, i.e., the difference of the activation barriers leading to the 4- and 5-substituted regioisomers and the corresponding yields. By comparing results from different protocols, we got insight into how post-CCSD(T) contributions, relativistic effects, and core-core/core-valence (CC/CV) electron interactions affect the regioisomeric ratio. The reference values were then compared to the values obtained by DFT calculations using a comprehensive set of density function approximations (DFAs) including meta-GGA, hybrid, and double hybrid DFAs, with and without dispersion correction, with respect to both the reaction energetics and isomeric ratio. The comparison allowed us to quantitatively assess DFAs as to their accuracy in predicting regioselectivity and to understand which factors affect the accuracy.

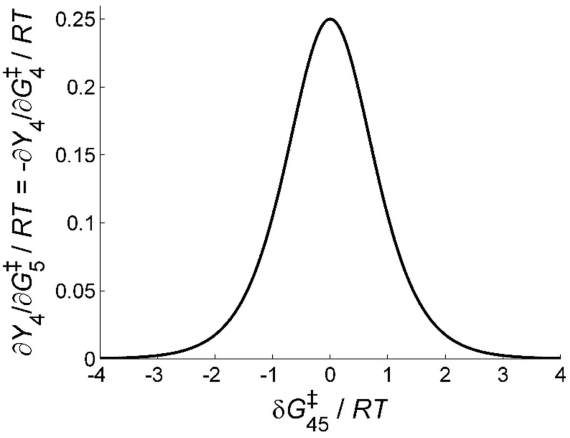

Figure 1. Plot of the sensitivity of the isomer yield Y_4 to the TS Gibbs energies $G_4^{\ddagger}$ and $G_5^{\ddagger}$. We recall that $\frac{\partial Y_4}{\partial G_5^{\ddagger}} = -\frac{\partial Y_4}{\partial G_4^{\ddagger}} = \frac{\partial Y_4}{\partial \delta G_{54}^{\ddagger}} = -\frac{\partial Y_4}{\partial \delta G_{45}^{\ddagger}}$.

Energetic Accuracy Analysis

As shown in the Supporting Information, in the framework of transition state (TS) theory, the yield Y_i of the *i*-th regioisomer of a given 1,3-DC only depends on the difference of the Gibbs free energies of the TSs leading to the two regioisomers (and, of course, on temperature *T*). For *i*, *j* = 4, 5 (regioisomeric TSs are denoted by the position of R, see Scheme 1), we can write

$$Y_i = \frac{1}{1 + \exp\left(-\frac{\delta G_{ji}^{\ddagger}}{RT}\right)} \tag{1}$$

where $\delta G_{ji}^{\ddagger} = G_j^{\ddagger} - G_i^{\ddagger}$ does not depend on the reactant free energies. Which accuracy of $G_i^{\ddagger}$ is required to calculate isomeric product yield with accuracy suitable for practical purposes? The sensitivity of Y_i to changes of the TS energetics is represented by the derivatives

$$\frac{\partial Y_4}{\partial G_4^{\ddagger}} = -\frac{\partial Y_4}{\partial G_5^{\ddagger}} = -\frac{1}{4RT}\,\mathrm{sech}^2\left(-\frac{\delta G_{45}^{\ddagger}}{2RT}\right) \tag{2}$$

and similar for Y_5. The sensitivity is largest when the two products form in equal amounts as in this case Equation (2) becomes

$$\frac{\partial Y_4}{\partial G_4^{\ddagger}} = -\frac{\partial Y_4}{\partial G_5^{\ddagger}} \approx -\frac{1}{4RT} \text{ for } \delta G_{45}^{\ddagger} \ll RT \tag{3}$$

And rapidly decreases for $\left|\delta G_{45}^{\ddagger}\right| \approx> RT$ (Figure 1).

For variations $\Delta G_i^{\ddagger} \ll G_i^{\ddagger}$, we can write $\Delta Y_i \approx \left(\frac{\partial Y_i}{\partial G_i^{\ddagger}}\right)\Delta G_i^{\ddagger}$ to estimate the energetic accuracy required in practical cases. In the $N = 2$ case, a 1% change in Y_4 corresponds to a change in either $G_4^{\ddagger}$ or $G_5^{\ddagger} \leq 0.04\ RT$, where the equal sign holds for $\delta G_{45}^{\ddagger} = 0$. To fix the order of magnitude, consider that an accuracy of 0.1 millihartree (mh) = 0.26 kJ/mol ensures that the computed isomer yield is in error by less than 3% throughout the 0–120 °C temperature range. The 0.1 mh threshold is conservative as it is estimated for the $\delta G_{45}^{\ddagger} \ll RT$ scenario that is the most demanding in terms of energetic accuracy. It is also conservative with respect to the number of isomers *N*. In the general case $N \geq 2$, the derivatives are largest when all $\delta G_{ji}^{\ddagger} \ll RT$ and can be expressed as

$$\frac{\partial Y_i}{\partial G_i^{\ddagger}} \approx \left(-\frac{1}{RT}\right)\frac{N-1}{N^2} \text{ and } \frac{\partial Y_i}{\partial G_j^{\ddagger}} \approx \left(-\frac{1}{RT}\right)\frac{1}{N^2} \tag{4}$$

The sensitivity (and therefore the required accuracy $\left|\Delta G_i^{\ddagger}\right|$ for a given $\left|\Delta Y_i\right|$ accuracy) is lower than that of the $N = 2$ case.

A more balanced choice for the energetic accuracy threshold can be made inspecting Figure 2, where the energetic accuracy required for a given Y_i accuracy (1 to 10%) between 0 and 120 °C is plotted for isomer ratio = 1:1 and 9:1.

An accuracy of 0.1 millihartree ensures that Y_i is in error by less than 3% for the 50:50 case and less than 1% for the 90:10 case throughout the considered temperature range. If we content ourselves with an accuracy of around 5% for the 50:50 case and better than 2% for the 90:10 case, the energetic accuracy threshold can be set at 0.2 mh = 0.53 kJ/mol. The latter accuracy is better than that conventionally required for reaction energies or barrier heights ('chemical accuracy': 1 kcal mol^{-1} ≈ 4 kJ mol^{-1} ≈ 1.6 mh) and comparable to that required for non-covalent interactions (0.1 kcal mol^{-1} ≈ 0.4 kJ mol^{-1} ≈ 0.16 mh).[44]

Is 0.1–0.2 mh accuracy achievable with present methods? Calculation of gas phase reaction barriers is certainly a formidable task, which has been central in computational chemistry. It involves the accurate evaluation of electronic energy and vibrational levels to calculate the partition function and Gibbs energy of the involved species. For reactions in solution, these terms must be evaluated using implicit or explicit solvent models. In this paper, we focus on the electronic energy term $\delta E_{ij}^{\ddagger} \equiv E_i^{\ddagger} - E_j^{\ddagger}$ in the Gibbs energy isomeric difference $\delta G_{ij}^{\ddagger}$ of gas-phase reactions. The former is the most

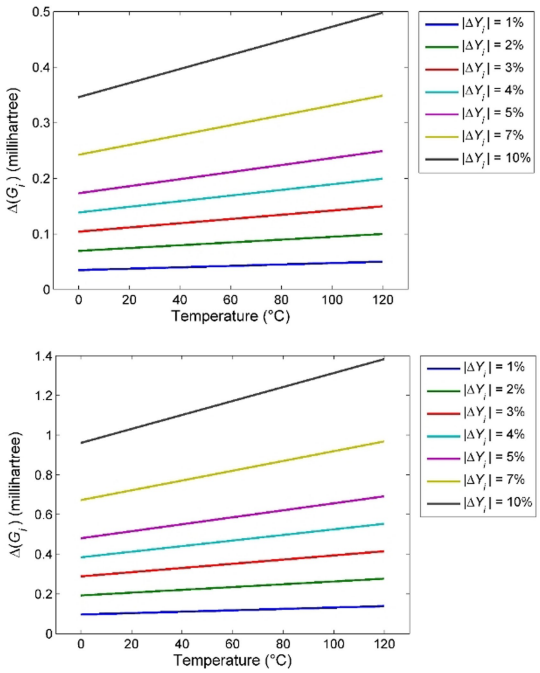

Figure 2. Energetic accuracy $|\Delta G_i^{\ddagger}|$ required for a given $|\Delta Y_i|$ accuracy (1 to 10%) between 0 and 120 °C. Isomer ratio is 1:1 (top, $\delta G_{45}^{\ddagger}=0$) and 9:1 [bottom, $\delta G_{45}^{\ddagger}=-RT\log(9)$].

demanding term as the calculation of accurate electronic energies requires high levels of theory and large basis sets in view of the slow convergence of the full configuration interaction (FCI) energy to the complete basis set (CBS) limit. The other contributions to the gas-phase Gibbs energy can usually be calculated at a lower level of theory than electronic energy.

High-level wavefunction (WF) based protocols, such as W4[45] and HEAT[46] are able to provide (gas phase) electronic energy reaction *barriers* $\Delta E^{\ddagger}=E_{TS}^{\ddagger}-\sum_{m=1}^{M}E_m$ with high accuracy (better than 0.1 kJ/mol ≈ 0.04 mh) but they can be applied only to very small systems due to their computational cost (e.g., W4 is based on FCI/CBS). W3-type protocols,[43] which include post-CCSD(T) contributions, can be applied to slightly larger systems but yield reaction barriers with accuracy not better than a few kJ/mol (≈1 mh) and thus seem unsuitable for the calculation of isomeric ratios. However, an important issue affecting the calculation of barrier heights is that reactants and TSs put different demands to the computational protocol used, because of factors such as the different convergence to the CBS limit,[47] and the unequal static correlation. So, the accuracy of $E_{TS}^{\ddagger}$ could in principle be better than that of the barrier $\Delta E^{\ddagger}$. Furthermore, the prediction of isomeric yields amounts to the calculation of energy *differences* between isomeric TSs ($\delta E_{ij}^{\ddagger}\equiv E_i^{\ddagger}-E_j^{\ddagger}$), which, from the electronic structure standpoint, are more similar to each other than to reactants thus enabling some error cancellation. These considerations suggest that accurate calculation of isomeric yields is not in principle impossible with present WF-based protocols and mainstream hardware, at least for small systems (≤6 heavy atoms). We note that the above discussion, including thresholds, is immediately translated to TS energy differences as, for $N=2$,

$$\frac{\partial Y_4}{\partial G_4^{\ddagger}}=-\frac{\partial Y_4}{\partial G_5^{\ddagger}}=\frac{\partial Y_4}{\partial \delta G_{45}^{\ddagger}}=-\frac{\partial Y_4}{\partial \delta G_{54}^{\ddagger}} \quad (5)$$

and similar for Y_5. Thus, accurate calculation of Y_i requires that $\delta E_{ij}^{\ddagger}$ is accurate to 0.1 or 0.2 mh.

For systems with more than 6 heavy atoms, one has to resort to DFT calculations. Among the very many DFAs available, recent benchmarking work has shown that (*i*) hybrid meta-GGA DFAs and hybrid GGA DFAs with large fractions of exact exchange reproduce *barrier* heights with accuracy not better than 7 kJ/mol = 2.7 mh,[16] and (*ii*) double-hybrid DFAs reach an accuracy of 5.4 kJ/mol = 2.1 mh.[48] These results are not so worse than W3-type results that an investigation about whether DFT calculations can be accurate enough to calculate isomeric yield is surely fruitless. Besides, dispersion correction can influence barrier heights by ≥4 kJ/mol.[44] and may further improve the DFT $\delta E_{ij}^{\ddagger}$. Although not an extremely promising working hypothesis, we decided to investigate whether DFT calculations, which are feasible for large systems, can be used to calculate isomeric yield with reasonable accuracy.

Our plan is as follows. We first calculate the energy difference $\delta E_{45}^{\ddagger}$ between TSs leading to the 4- and 5-susbstituted regioisomers and the regioisomeric yield Y_4 ($Y_5=1-Y_4$) of these 12 cycloadditions by using WF-based protocols. The 4-susbstituted regioisomers is favored ($Y_4>Y_5$) when $\delta E_{45}^{\ddagger}<0$. In the lack of high-quality gas-phase data for the above reactions, we use the WF-based protocol results as reference values to rank DFAs. Besides, by comparing results from different protocols, we get insight into how post-CCSD(T) contributions, relativistic effects, and core-core/core-valence (CC/CV) electron interactions affect the regioisomeric ratio. Next, $\delta E_{45}^{\ddagger}$ and Y_4 are calculated using a comprehensive set of meta-GGA, hybrid, and double hybrid DFAs and dispersion corrections using the D3,[49,50] D3-BJ,[50,51] and D4[52] methods. The DFT results are compared to the benchmark values to assess their accuracy in predicting the regioselectivity and understand which factors affect the accuracy.

Results and Discussion

Wavefunction Based Protocols

We computed the electronic energy of the TSs leading to the 4- and 5-substituted products of the 1,3-DC of HN_3 with the alkynes HC≡C–R and alkenes H_2C=CH–R (R=F, OH, NH_2, Me, CN, CHO). The choice of the substituent R was dictated by the conflicting demands of reasonable computational cost of high-level protocols and suitable coverage of the "reaction" space (see Methods Section). We used the protocols W1BD,[53] W1X-1,[54] W1-F12,[13] W2X,[55] W2-F12,[13] WMS,[56] and W3X.[57] More advanced W3 protocols (such as W3X-L,[55] W3lite-F12,[35] W3-F12[13]) required excessive storage resources because of the larger basis sets involved. In a nutshell, the above listed

protocols rely on several frozen-core (FC) non-relativistic (NR) CCSD(T) calculations to estimate the FC NR CCSD(T) electronic energy at the CBS limit, except for W1BD that relies on a Brueckner Doubles calculation with triples excitations.[58] They include different core-core/core-valence (CC/CV) and relativistic corrections. W3-type protocols also include post-CCSD(T) contributions from exact triple and perturbative quadruple excitations. Therefore, for the following discussion, we take W3X protocol as a reference. The reader is referred to a synoptic comparison of these protocols[43] and to the above cited articles for details.

In Table 1, the energetic differences $\delta E_{45}^{\ddagger}$ between the TSs leading to the 4- and 5-substituted regioisomers are collected. For a more practical view of the results, we collected in Table 2 the yield Y_4 of the 4-substituted regioisomer, calculated from $\delta E_{45}^{\ddagger}$ assuming room temperature (r.t., $T = 298$ K). First, we consider the results calculated by the highest-level protocol, i.e., W3X. Our reaction set spans a wide range of Y_4 from 99.5 to 0.2% (equivalent to a $\delta E_{45}^{\ddagger}$ range of 10.7 mh = 28.0 kJ/mol^{-1}). In addition to high regioselectivity cases, our reaction set entails difficult cases with low regioselectivity ($\delta E_{45}^{\ddagger} \cong RT = 0.944$ mh at r.t.), for example, R=Me, showing that it adequately covers the chemical space. Some substituents favor the same regioisomer for both the alkyne and alkene dipolarophile: F favors the 5-substituted product, while R=CHO and CN favor the 4-susbstituted one. In the presence of R=Me, NH_2, and OH, different regioisomeric products are favored depending upon the alkenyl or alkynyl nature of the dipolarophile. Regioselectivities higher than 90% are calculated in both alkynes and alkenes for R=F and NH_2. Curiously, in the latter case the regioselectivity outcome is opposite in the two dipolarophile classes (Tables 1 and 2). High regioselectivity is also predicted for HC≡C–OH and H_2C=CH–CN. In the other cases, especially for R=Me, low levels of regioselectivity are predicted. It is note-

Table 1. Differences $\delta E_{45}^{\ddagger}$ between the TSs leading to the 4- and 5-substituted regioisomers. The statistics of the $\delta E_{45}^{\ddagger} - \delta E_{45}^{\ddagger}$(W3X) difference are collected at the bottom of the Table. All values are in millihartree.

	R	W1BD	W1X-1	W1-F12	W2X	W2-F12	WMS	W3X
HC≡C–R	CHO	−0.870	−0.813	−0.886	−0.870	−0.896	−0.915	−0.885
	CN	−0.419	−0.386	−0.454	−0.438	−0.474	−0.401	−0.432
	F	4.263	4.188	4.263	4.279	4.275	4.260	4.100
	Me	−0.338	−0.268	−0.286	−0.249	−0.260	−0.294	−0.405
	NH_2	−5.141	−5.013	−4.998	−4.904	−4.905	−5.133	−4.916
	OH	−2.106	−2.098	−2.078	−2.067	−2.056	−2.101	−2.257
H_2C=CH–R	CHO	−0.956	−0.987	−1.027	−1.042	−1.068	−1.087	−0.994
	CN	−2.949	−2.944	−3.009	−3.021	−3.062	−3.073	−2.928
	F	4.161	4.106	4.167	4.218	4.222	4.150	3.985
	Me	0.319	0.437	0.499	0.488	0.507	0.439	0.312
	NH_2	5.805	5.827	5.952	6.008	6.043	5.903	5.741
	OH	1.319	1.343	1.416	1.486	1.492	1.432	1.128
	MSD[a]	0.053	0.079	0.092	0.120	0.114	0.061	
	RNG	0.416	0.312	0.370	0.451	0.497	0.521	
	MAX[b]	0.225	0.215	0.287	0.357	0.364	0.303	
	MAD[c]	0.094	0.097	0.129	0.144	0.158	0.142	

[a] Mean signed deviation. [b] Maximum absolute deviation. [c] Mean absolute deviation.

Table 2. Yield Y_4 of the 4-substituted regioisomer. The statistics of the $Y_4 - Y_4$(W3X) difference are collected at the bottom of the Table. All values are in %.

	R	W1BD	W1X-1	W1-F12	W2X	W2-F12	WMS	W3X
HC≡C–R	CHO	71.5	70.3	71.9	71.5	72.1	72.5	71.9
	CN	60.9	60.1	61.8	61.4	62.3	60.5	61.2
	F	1.1	1.2	1.1	1.1	1.1	1.1	1.3
	Me	58.9	57.1	57.5	56.6	56.8	57.7	60.6
	NH_2	99.6	99.5	99.5	99.4	99.4	99.6	99.5
	OH	90.3	90.2	90.0	89.9	89.8	90.2	91.6
H_2C=CH–R	CHO	73.4	74.0	74.8	75.1	75.6	76.0	74.1
	CN	95.8	95.8	96.0	96.1	96.2	96.3	95.7
	F	1.2	1.3	1.2	1.1	1.1	1.2	1.4
	Me	41.6	38.6	37.1	37.3	36.9	38.6	41.8
	NH_2	0.2	0.2	0.2	0.2	0.2	0.2	0.2
	OH	19.8	19.4	18.3	17.2	17.1	18.0	23.2
	MSD[a]	−0.7	−1.2	−1.1	−1.3	−1.2	−0.9	
	RNG	3.5	3.9	5.7	7.0	7.6	7.1	
	MAX[b]	3.4	3.8	5.0	6.1	6.2	5.2	
	MAD[c]	0.7	1.3	1.4	1.6	1.7	1.4	

[a] Mean signed deviation. [b] Maximum absolute deviation. [c] Mean absolute deviation.

worthy that the qualitative regioselectivity predictions about the $HN_3 + H_2C{=}CH{-}R$ 1,3-DCs based on the W*n* protocols agree, not only with recent B3LYP results,[12] but also with those based on the CNDO/2 MO coefficients published 50 years ago and the experimental data therein cited.[6,7]

The indication of the major regioisomer, i.e., the sign of $\delta E^{\ddagger}_{45}$ is the same for all W*n* protocols (this qualitative agreement holds also when CC/CV and Rel contributions to $\delta E^{\ddagger}_{45}$ are neglected) and $\delta E^{\ddagger}_{45}$ is similar across the W*n* protocols. Comparison of the protocols allows us to understand their effectiveness and, exploiting their composite nature, to investigate which energy contributions are important to accurately compute $\delta E^{\ddagger}_{45}$.

As statistical indices, we use the mean absolute deviation (MAD), the maximum absolute deviation (MAX), the range of signed deviations (RNG), and the mean signed deviation (MSD). The W*n* methods tend to favor the 5-substituted isomer with respect to W3X (i.e., more positive $\delta E^{\ddagger}_{45}$), especially for alkene dipolarophiles, as also shown by the statistics of the $\delta E^{\ddagger}_{45} - \delta E^{\ddagger}_{45}$(W3X) difference (Table 1). The MSD, which highlights systematic effects, ranges from +0.053 (W1BD) to +0.120 mh (W2X). The MAD ranges from 0.094 (W1BD) to 0.158 mh (W2-F12). The full range (RNG) of $\delta E^{\ddagger}_{45} - \delta E^{\ddagger}_{45}$(W3X) however is between 0.312 (W1X-1) and 0.521 mh (WMS), suggesting that the post-CCSD(T) corrections in W3X are important for the accurate calculation of $\delta E^{\ddagger}_{45}$. The MSD of the $Y_4 - Y_4$(W3X) difference (Table 2) is of course negative, indicating the presence of systematic effects generally favoring the Y_5 isomer. Both |MSD| and MAD are below 2%. The maximum deviation from Y_4(W3X) ranges from 3.4% to 6.2%. As expected, the maximum distance occurs when the Y_4 is not far from 50% (R=Me, OH). In conclusion, accurate isomeric ratios require inclusion of exact triple and perturbative quadruple excitations but when an error up to 4% is acceptable, cheaper alternatives are available, such as W1BD and W1X-1.

Energetic Contributions to $E^{\ddagger}_i$ and $\delta E^{\ddagger}_{45}$ in W3X Protocol

We now consider the energetic contributions to $E^{\ddagger}_i$ and $\delta E^{\ddagger}_{45}$ in the W3X protocol. $E^{\ddagger}_i$(W3X) is based on the frozen-core, non-relativistic CCSD(T) energy, corrected by CC/CV, relativistic, and post-CCSD(T) (exact triple and perturbative quadruple excitations) contributions* (*W3X protocol computes CC/CV and Rel simultaneously as the difference between a full-electron relativistic and a frozen-core non-relativistic MP2/cc-pCVTZ calculations. We split the CC/CV and Rel contributions using a full-electron non-relativistic MP2/cc-pCVTZ calculation to compute the CC/CV contribution. Then, the Rel contribution was obtained by subtracting the latter from the total CC/CV + Rel correction) The contributions $E^{\ddagger}_i(C)$ to $E^{\ddagger}_i$ are shown in the boxplots in Figure 3 and summarized in Table 3 as averages over the 24 isomeric TSs.

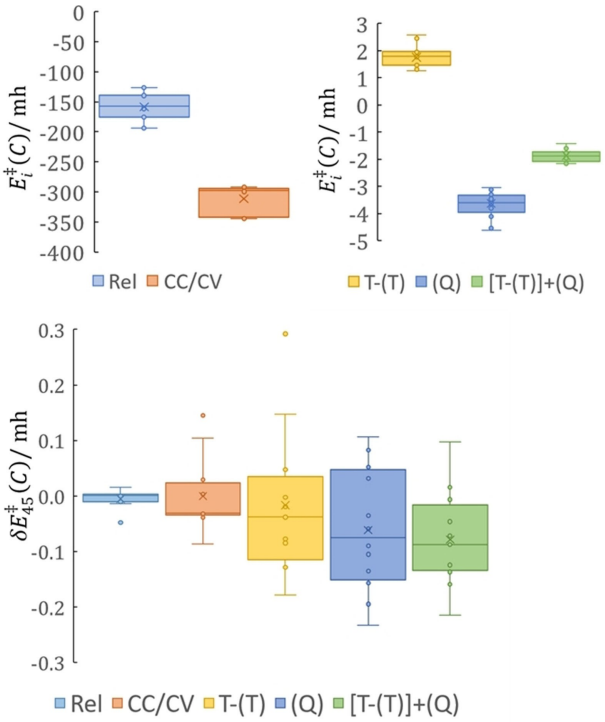

Figure 3. Absolute energetic contributions $E^{\ddagger}_i(C)$ (top) and $\delta E^{\ddagger}_{45}(C)$ (bottom), additional to CCSD(T), of W3X protocol. Note the different vertical scales in the subpanels.

Of course, the CCSD(T) energy is by large the dominating term, contributing more than 99.8% of $E^{\ddagger}_i$. Both CC/CV and Rel contributions amount to a few hundred mh, and the post-CCSD(T) contribution to a few mh, also because the effect of including exact triples T−(T) [$E_{CCSDT} - E_{CCSD(T)}$] and perturbative quadruples (Q) [$E_{CCSDT(Q)} - E_{CCSDT}$] are of similar size and opposite

Table 3. Energetic contributions $E^{\ddagger}_i(C)$ and $\delta E^{\ddagger}_{45}(C)$ of W3X protocol. Values are averaged over the 24 isomeric TSs; standard deviation in parentheses. The scaling factors are given as intervals.

C	$\langle E^{\ddagger}_i(C)\rangle$[a] [mh]	$\langle E^{\ddagger}_i(C)/E^{\ddagger}_i\rangle$[b] [%]	$\langle\lvert\delta E^{\ddagger}_{45}(C)\rvert\rangle$[c] [mh]	$E^{\ddagger}_i(C) \rightarrow \delta E^{\ddagger}_{45}(C)$ scaling factor[d]
W3X	280–355 10^3	100	−4.92–+5.74	10^{-5}–10^{-6}
CCSD(T)	280–355 10^3	99.853(2)	−4.94–+5.77	10^{-5}–10^{-6}
CC/CV	−312(62)	0.097(5)	0.048	10^{-4}–10^{-5}
Rel	−160(22)	0.049(4)	0.010	10^{-4}–10^{-6}
T−(T)	1.7(3)	−5(1) 10^{-4}	0.098	10^{-1}–10^{-2}
(Q)	−3.6(4)	11(1) 10^{-4}	0.107	10^{-1}–10^{-2}
[T−(T)] + (Q)	−1.9(2)	5.8(4) 10^{-4}	0.097	10^{-1}–10^{-2}

[a] For W3X and CCSD(T), the $E^{\ddagger}_i(C)$ range is reported. [a] Relative to $E^{\ddagger}_i$(W3X). [c] For W3X and CCSD(T), the $\delta E^{\ddagger}_{45}(C)$ range is reported. [d] The scaling factor is defined as $2\,\delta E^{\ddagger}_{45}(C)/\left[E^{\ddagger}_4(C) + E^{\ddagger}_5(C)\right]$ for each energetic contribution.

sign. The Total Atomization Energy TAE[(T)] diagnostic[45] (Table S1) is in the range 3.5–4.9% and 3.0–3.8% for TSs involving alkynes and alkenes, respectively, indicating that non-dynamical correlation effects are on the high side of the "mild" region (<5%).[14] Post-CCSD(T) contributions to $E_i^{\ddagger}$ are then expected to be 0.8 to 1.6 mh (2 to 4 kJ/mol),[43] a slight underestimation when compared to the [T−(T)]+(Q) corrections computed for our reaction set within the W3X protocol (Table S2). The TAE[(T)] difference between isomeric TSs is minor.

Taking the difference $\delta E_{45}^{\ddagger}$ involves the large energy cancellation typical of quantum chemistry, and this cancellation dramatically changes the relative importance of the contributions. The contributions $\delta E_{45}^{\ddagger}(C)$ are shown in the boxplots in Figure 3 and collected in Tables S3-S6 in the Supporting Information, where a more detailed discussion of the energetic contributions can be found. Each $\delta E_{45}^{\ddagger}(C)$ can be either positive or negative, depending on the reaction, and we note that [T−(T)] and (Q) contributions have unequal sign in 7 reactions out of 12. The reaction-averaged absolute value $\left|\delta E_{45}^{\ddagger}(C)\right|$ are collected in Table 3. In addition to the obvious preponderance of the CCSD(T) contribution, one can see that the post-CCSD(T) contribution (≈0.1 mh) is now more important than the CC/CV and Rel corrections. The latter ones (especially Rel) are core-centered contributions and substantially cancel in the calculation of $\delta E_{45}^{\ddagger}$, as shown by the very small $E_i^{\ddagger}(C) \rightarrow \delta E_{45}^{\ddagger}(C)$ scaling factor (Table 3), which measures how much a given contribution decreases from $E_i^{\ddagger}$ to $\delta E_{45}^{\ddagger}$. The post-CCSD(T) contribution scales by a factor 10^{-1}–10^{-2}, several orders of magnitude larger than that of CC/CV, Rel, and CCSD(T) energies. The low scaling factor shows that the post-CCSD(T) contribution is closely linked to the ongoing chemistry and that accurate description of electron correlation is important for regioselectivity, as anticipated by the comparison of the W*n* protocols.

This discussion has shown that neglecting post-CCSD(T) contributions to $\delta E_{45}^{\ddagger}$ can cause errors in calculated isomeric ratios ≈5%. These contributions are important to accurately describe to the ongoing chemistry and do not benefit from important cancellation between isomeric TSs (conversely to CC/CV and Rel contributions). Similar to $E_i^{\ddagger}$, when evaluating $\delta E_{45}^{\ddagger}$, calculation of the [T−(T)] correction alone is not advisable since it often has sign opposite to the (Q) correction.

DFT Calculations

Our question is: how accurate are DFAs in calculating $\delta E_{45}^{\ddagger}$ and Y_4? In other words, can DFT calculations be used in place of expensive W*n* protocols to extend the scope of computable isomeric ratios beyond the simplest systems?

We calculated $\delta E_{45}^{\ddagger}$ and Y_4 using meta-GGA, hybrid, and double hybrid DFAs that are pre-defined in Gaussian16 A.03[59] and ORCA 4.2.1,[60,61] using the pcseg-3 basis set,[62] and the recent neural-network-trained DeepMind 21 (DM21) DFA.[63] The latter can be described as a local range-separated hybrid DFA. DFAs are here classified as meta-GGA (both non empirical and semi-empirical DFAs considered), hybrid (comprising both GGA and meta-GGA. both non empirical and semi-empirical, and both global and range-separated DFAs), and double-hybrid (comprising both global and range-separated DFAs). When dispersion is not integral part of the DFA definition and dispersion parameters are available, we computed D3,[49,50] D3BJ,[49,50] D4,[52] and VV10[64] dispersion corrections. Inclusion of dispersion led to 68 combinations of DFA and dispersion correction.

Our plan to assess the DFAs is as follows. We first consider purely KS-SCF electronic energies, i.e., DFAs without dispersion correction and rank the DFA according to the difference $\delta E_{45}^{\ddagger}-\delta E_{45}^{\ddagger}$(W3X). Such "theory-oriented" assessment will allow us to find out which characteristics are typical of the DFAs best approximating the reference $\delta E_{45}^{\ddagger}$(W3X). Using several measures to rank the DFAs, i.e., MSD, MAD, MAX, and RNG of $\delta E_{45}^{\ddagger}-\delta E_{45}^{\ddagger}$(W3X) for the 12 1,3-DCs (see Methods Section), will further improve the robustness of our conclusions. Next, we augment the set of $\delta E_{45}^{\ddagger}$ with values obtained using (i) DFAs containing a dispersion correction as part of their definition and (ii) all combinations of DFA and dispersion correction made possible by the availability of D3, D3BJ, D4, and VV10 parameters. This larger set is compared to the reference values of both $\delta E_{45}^{\ddagger}$ and Y_4. Such "practice-oriented" assessment will allow us to ascertain the importance of dispersion correction, to rank DFA +dispersion combinations with respect to both theoretical ability ($\delta E_{45}^{\ddagger}$) and practical prediction (Y_4), and to recommend the best combination. Furthermore, using both $\delta E_{45}^{\ddagger}-\delta E_{45}^{\ddagger}$(W3X) and Y_4-Y_4(W3X) improves the robustness of our ranking and recommendation.

KS-SCF Electronic Energies

We begin with the analysis of DFT KS-SCF electronic energies. Excluding DFAs with integrated dispersion (e.g., ωB97M–V), we used 91 DFAs pre-defined in Gaussian16 or ORCA and dispersion-free DM21. The $\delta E_{45}^{\ddagger}-\delta E_{45}^{\ddagger}$(W3X) of nominally equal DFAs from Gaussian16 and ORCA turned out to differ less than 0.04 mh for each reaction and were considered identical, except for O3LYP. Our set thus decreased to 77 unique DFAs.

In Figure 4, these DFAs are ranked by the MSD and MAD of $\delta E_{45}^{\ddagger}-\delta E_{45}^{\ddagger}$(W3X) of the 12 considered 1,3-DC reaction (see Figure S1 for bar charts of MAX and RNG). The MSD is positive, except for M06-HF,[65] indicating that (on average) DFAs excessively favor the 5-substituted product. In view of the behavior of W1- and W2-type protocols, this can be ascribed to inaccurate description of electron correlation. DM21 has the lowest systematic error and the non-hybrid meta-GGA DFAs generally have the highest one. Double-hybrid DFAs are interspersed with the hybrid DFAs, but it is the latter ones (especially the range-separated DFAs) that rank just below DM21. Looking at the individual reactions (Figure S2), one however sees that the DFAs over-favor the 5-substituted isomer for R=Me, NH_2, OH, F but they oppositely behave for R=CHO and CN. The bar charts of MAD, MAX, and RNG show a similar shape. Starting from the lower end, the deviation decreases steadily, then reaches a plateau, and finally there is a marked

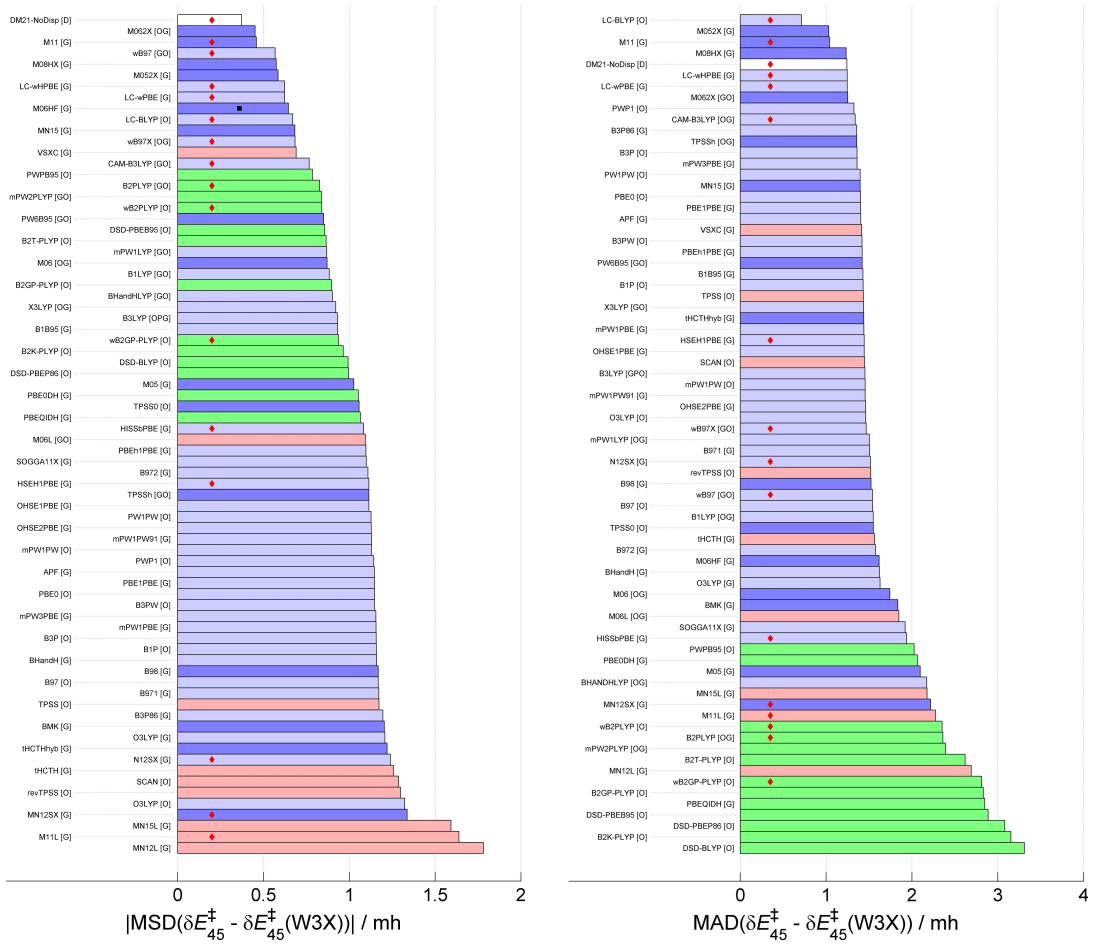

Figure 4. Mean signed (MSD) and mean absolute (MAD) difference $\delta E^{\pm}_{45} - \delta E^{\pm}_{45}$(W3X) calculated using DFAs with no dispersion. The letter(s) in square brackets denote the software package. Red: meta-GGA DFAs; light blue: hybrid GGA DFAs; dark blue; hybrid meta-GGA DFAs; green double-hybrid DFAs; white: DM21. Red diamonds indicate range-separated DFAs. The black dot in the MSD bar chart indicates that M06-HF has negative MSD.

decrease for the few best DFAs. Double-hybrid DFAs cluster towards large deviations from the W3X reference, which is somewhat surprising in view of the reported accuracy of double-hybrid DFAs.[14,48] The poor performance of double hybrids could be due their slow basis set convergence inherited from MP2.[66] Among the hybrid DFAs, GGA hybrids occupy most of the top half and meta-GGA hybrids are found throughout the deviation range but the best ones cluster at the high accuracy end, in agreement with their performance in the calculation of barrier heights.[16] Non-hybrid meta-GGA DFAs are mostly found towards in the worst half, but they include some noteworthy results, for example, VSXC[67] (MAD) and SCAN[68] (MAX, RNG). SCAN, corrected for dispersion by D3BJ, was among the finally recommended DFAs, based on the GMTKN55 database.[69] Range-separated DFAs (marked by a red diamond in Figure 4) are on average better than the global DFAs of the same type, for example, compare B3LYP with CAM-B3LYP. A similar conclusion has been recently drawn for Diels–Alder reactions.[70] Double-hybrids are not suited for the calculation of dispersion-uncorrected $\delta E^{\pm}_{45}$ for our 1,3-DC reaction set. Range-separated hybrid DFAs are required for accurate $\delta E^{\pm}_{45}$, which strongly suggests that accurate treatment of exchange and correction of the self-interaction error at the interatomic distances typical of breaking/forming bonds, is of fundamental importance,[69] as also supported by the MSD sign of M06-HF.

We now focus on the 15 best-performing DFAs for MAD, MAX, and RNG statistics (Table 4). All statistics indicate that the investigated DFAs are not able to reproduce the reference $\delta E^{\pm}_{45}$ with the desired accuracy. Being the best MAD $\approx$0.7 mh, one might conclude that one should expect an accuracy of Y_4 slightly better than 20% in the demanding 50:50 case and better than 7% in the 90:10 case (Figure 2). Looking at MAX and RNG, it would seem that accuracy is worse in some cases. However, we recall that the effect of $\delta E^{\pm}_{45}$ inaccuracy on Y_4 is very sensitive to $\delta E^{\pm}_{45}$ itself (Figure 1).

The three sets of the 15 best performing DFAs share 9 DFAs (bold in Table 4), which consistently rank among the 11 best ones, often with similar ranking. These 9 DFAs perform well in a robust way, i.e., independent of the considered statistics. They belong to the two families of range-separated hybrids and Minnesota meta-GGA hybrids, again showing the importance of the correction of the self-interaction error and description of electron exchange. Range-separated GGA hybrid LC-BLYP[71] has the lowest MAD and RNG but has relatively large MAX (ranks

Table 4. The 15 top-ranking DFAs with respect to the MAD, MAX, and RNG statistics for the $\delta E^{\pm}_{45} - \delta E^{\pm}_{45}$(W3X) difference. The DFAs highlighted in bold occur in all three subsets.

MAD [mh]		MAX [mh]		RNG [mh]	
1.397	PW1PW	4.362	B1B95	5.253	MN15
1.362	mPW3PBE	4.265	PW6B95	5.217	B3P86
1.361	B3P	4.191	ωB97X	5.190	PWP1
1.357	TPSSh	4.158	ωB97	5.170	mPW3PBE
1.357	B3P86	4.134	**CAMB3LYP**	5.153	B3P
1.339	**CAMB3LYP**	4.108	MN15	5.138	**CAMB3LYP**
1.326	PWP1	3.709	**LC-ωPBE**	5.111	**LC-ωPBE**
1.253	**M06-2X**	3.707	**LC-ωHPBE**	5.109	**LC-ωHPBE**
1.247	**LC-ωPBE**	3.534	M06HF	5.058	SCAN
1.247	**LC-ωHPBE**	3.242	**LC-BLYP**	4.855	**DM21-NoDisp**
1.244	**DM21-NoDisp**	3.223	**DM21-NoDisp**	4.294	**M11**
1.235	**M08HX**	3.220	**M11**	4.229	**M08HX**
1.041	**M11**	2.969	**M08HX**	3.985	**M06-2X**
1.031	**M05-2X**	2.834	**M05-2X**	3.601	**M05-2X**
0.713	**LC-BLYP**	2.606	**M06-2X**	3.492	**LC-BLYP**

6th, with MAX 0.636 mh higher than M06-2X). The four Minnesota DFAs rank very high, they are outperformed only by LC-BLYP for the MAD and RNG statistics. M05-2X,[72] M06-2X,[73] and M08-HX[74] are meta-GGA global hybrids with 56%, 54%, and 52% of exact exchange while M11[75] is a range-separated meta-GGA hybrid with 43% exact exchange. The dispersion-uncorrected version of DM21 comes next and is followed by other range-separated GGA hybrids LC-ωHPBE,[76] LC-ωPBE,[77] and CAM-B3LYP.[78] In their dispersion corrected form, M05-2X ranked 3rd in the subset of hybrid DFAs when assessed against the updated BHPERI dataset,[14] and M08-HX and ωB97X were among the best three hybrids when assessed against the BH subset of GMTKN55.[69] M11 was among the best five DFAs proposed for Diels–Alder reaction barrier height and regioselectivity when assessed against CCSD(T)/CBS data.[70]

We also investigated how the ranking of DFAs without dispersion correction depends on the reference protocol (Tables S7–S9). The analysis detailed in the Supporting Information confirm the importance of the [T−(T)] and (Q) contribution for the accurate calculation of $\delta E^{\pm}_{45}$. Nine DFAs are consistently among the best-15 DFAs irrespective of statistics and reference. They are CAM-B3LYP, DM21-NoDisp, LC-BLYP, LC-ωHPBE, LC-ωPBE, M05-2X, M06-2X, M08-HX, and M11 (in alphabetical order). The ranking depends on the statistics and reference, but it is noteworthy that LC-BLYP is the best ranking DFA in all cases, except for the MAX statistics relating to the W3X and W1X-1 protocols.

Dispersion Corrected Energies and Regioisomeric Yield

We now include the dispersion corrections in our analysis. The $\delta E^{\pm}_{45}$ dataset is augmented with DFAs containing a dispersion correction as part of their definition (25 DFAs) plus all combinations of DFA and dispersion correction made possible by the availability of D3, D3BJ, D4, and VV10 parameters. We used 185 DFAs pre-defined in Gaussian16 or ORCA and DM21. Using the same threshold of 0.04 mh as for the KS-SCF energies, 24 nominally equal (including dispersion) DFAs resulted equivalent, and our set decreased to 162 unique DFAs.

In Figure 5, these DFAs are ranked by the MSD and MAD of $\delta E^{\pm}_{45} - \delta E^{\pm}_{45}$(W3X) of the 12 considered 1,3-DC reaction (see Figure S3 for bar charts of MAX and RNG). The MSD graph is similar to that of DFAs without dispersion. MSD is positive, except for M06-HF and M06-HF + D3, showing excessive preference for the 5-substituted isomer. The full formulation of DM21, which includes D3BJ dispersion, has the lowest systematic error. The behavior of the various DFA classes and the substituent-dependent preference are not much different from those displayed by the dispersion-uncorrected DFAs. The MAD, MAX, and RNG graphs also have the same general appearance as those of DFAs without dispersion have. Double-hybrid DFAs unexpectedly[14,48] cluster towards large deviations. Even when dispersion-corrected, double-hybrids are not suited for the calculation of $\delta E^{\pm}_{45}$. GGA hybrids occupy most of the range center-top and several meta-GGA hybrids are found at the high accuracy end, in agreement with their performance in the calculation of barrier heights.[16] Non-hybrid meta-GGA DFAs are found in the worse half. Range-separated DFAs are in general better than the global DFAs of the same type. Range-separated hybrid DFAs, especially when dispersion-corrected, are needed to minimize the difference from the reference, which strongly suggests that accurate treatment of interactions at the interatomic distances typical of breaking/forming bonds is of fundamental importance.

Functional with integrated dispersion terms tend to perform better than the corresponding dispersion-uncorrected DFAs. In most (but not all) cases, any type of dispersion correction is beneficial (Table S10). However, Figure 5 and Table 5 show that about only 10 out of the best 15 DFAs include dispersion correction. The best MAD is still displayed by LC-BLYP whereas the beneficial effect of dispersion correction on large $\delta E^{\pm}_{45} - \delta E^{\pm}_{45}$(W3X) values makes ωB97M-D3BJ the best DFA as to the MAX and RNG statistics (Figure S3). The improvement over the dispersion-uncorrected DFAs is however not large: −0.270 mh for MAX and −0.081 mh for RNG. This minor impact of dispersion correction on the $\delta E^{\pm}_{45}$ accuracy is probably due to

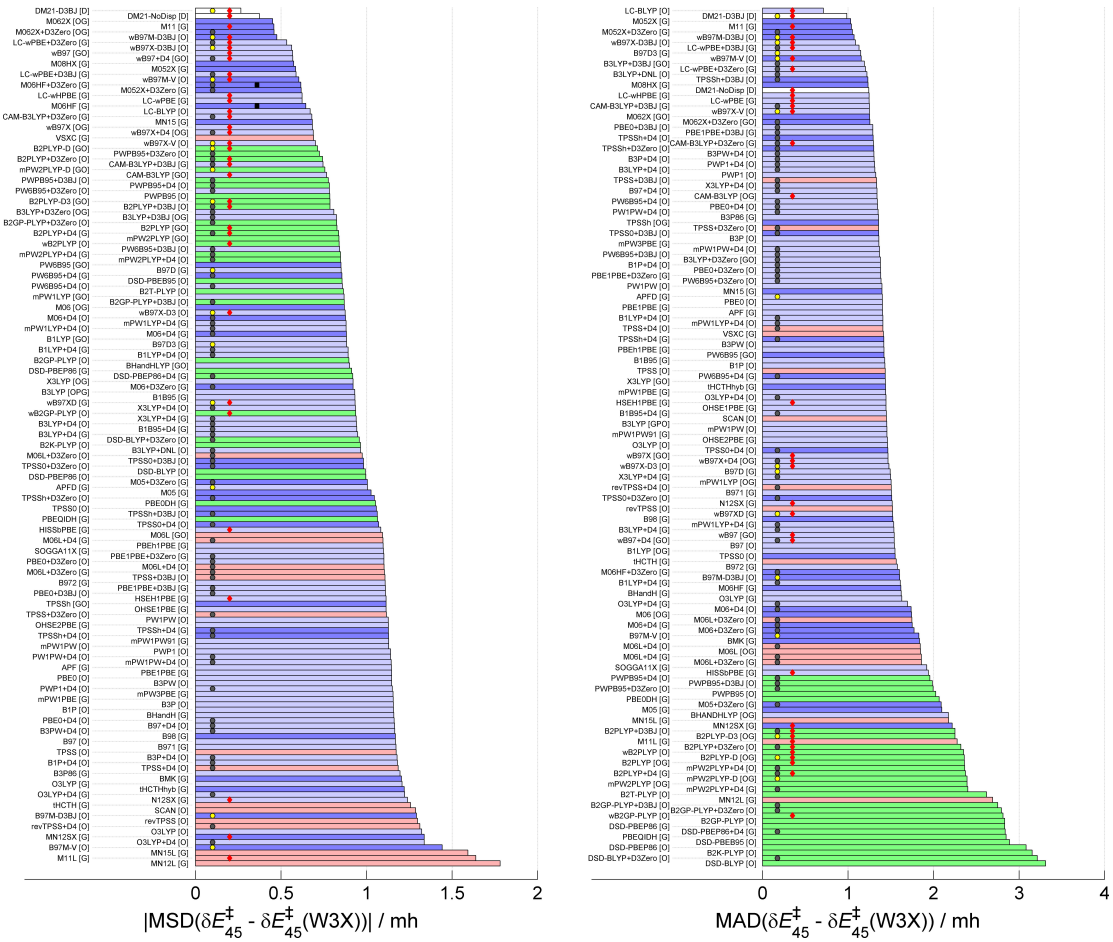

Figure 5. Mean signed (MSD) and mean absolute (MAD) difference $\delta E^{\ddagger}_{45} - \delta E^{\ddagger}_{45}$(W3X) calculated using all DFAs. The letter(s) in square brackets denote the software package. Red: meta-GGA DFAs; light blue: hybrid GGA DFAs; dark blue; hybrid meta-GGA DFAs; green: double-hybrid DFAs; white: DM21. Additional information about the DFA type is given by symbols. Yellow dot: DFA including dispersion correction, gray dot: dispersion-corrected DFA. Red diamonds: range-separated DFA. The black dots in the MSD bar chart indicate that M06-HF and M06-HF + D3 have negative MSD.

Table 5. The 15 top-ranking DFAs with respect to the MAD, MAX, and RNG statistics for the $\delta E^{\ddagger}_{45} - \delta E^{\ddagger}_{45}$(W3X) difference. The DFAs highlighted in bold occur in all three subsets. The underlined DFAs are the best-ranking DFAs in Table 4.

MAD [mh]		MAX [mh]		RNG [mh]	
1.235	**M08-HX**	3.466	M06HF + D3Zero	4.712	CAM-B3LYP + D3BJ
1.233	TPSSh + D3BJ	3.287	**LC-ωPBE + D3BJ**	4.689	**LC-ωPBE + D3**
1.222	B3LYP + DNL	3.243	**LC-ωPBE + D3**	4.565	**LC-ωPBE + D3BJ**
1.204	**LC-ωPBE + D3**	3.242	**LC-BLYP**	4.546	ωB97X-V
1.192	B3LYP + D3BJ	3.223	DM21	4.294	**M11**
1.156	**ωB97 M-V**	3.220	**M11**	4.229	**M08-HX**
1.150	B97 + D3	2.986	**ωB97 M-V**	3.993	M06-2X + D3
1.129	**LC-ωPBE + D3BJ**	2.969	**M08-HX**	3.985	M06-2X
1.088	**ωB97X-D3BJ**	2.893	**M05-2X + D3**	3.974	**ωB97 M-V**
1.072	**ωB97M-D3BJ**	2.834	**M05-2X**	3.739	**ωB97X-D3BJ**
1.051	**M05-2X + D3**	2.668	**ωB97X-D3BJ**	3.703	**DM21-D3BJ**
1.041	**M11**	2.624	M06-2X + D3	3.628	**M05-2X + D3**
1.031	**M05-2X**	2.606	M06-2X	3.601	**M05-2X**
0.986	**DM21-D3BJ**	2.339	**DM21-D3BJ**	3.492	**LC-BLYP**
0.713	**LC-BLYP**	2.336	**ωB97M-D3BJ**	3.413	**ωB97M-D3BJ**

fact that it is largely cancelled when the isomeric TS energy difference $\delta E^{\ddagger}_{45}$ is calculated. In our systems, the mean dispersion correction to the TS energy $E^{\ddagger}_{i}$ is less (in absolute value) than 10 mh (maximum ≈20 mh) but the mean contribution of dispersion to $\delta E^{\ddagger}_{45}$ is less (in absolute value) than 0.1 mh (maximum ≈0.8 mh). Since the best statistics have little (if any) changed with respect to the case of dispersion-uncorrected DFAs, so is the conclusion that the investigated DFAs seem to

be unable to reproduce the reference $\delta E_{45}^{\pm}$ with the desired accuracy. However, we recall that the effect of $\delta E_{45}^{\pm}$ inaccuracy on Y_4 is very sensitive to $\delta E_{45}^{\pm}$ itself (Figure 1) and we next investigate the ability of DFAs to reproduce the regioisomeric yield Y_4.

Before that, we briefly analyze the rankings in Table 5. The three sets of the 15 top-ranking DFAs share 11 DFAs, 7 of which include dispersion correction. This shows that they perform well in a robust way, i.e., independent of the considered statistics. The ranking, however, strongly depends on the statistics. The 11 common DFAs belong to the two families of range-separated hybrids and Minnesota meta-GGA hybrids, again showing the importance of the correction of the self-interaction error and description of electron exchange. Range-separated GGA hybrid LC-BLYP[71] has the lowest MAD and next-to-lowest RNG, but it has relatively large MAX (ranks 12th). The similar LC-ωPBE[77] ranks 8th–14th when dispersion-corrected by D3 or D3BJ. ωB97M-D3BJ[79,80] has the lowest MAX and RNG but its expected absolute error (MAD) is 0.359 mh higher than that of LC-BLYP. The similar ωB97 M-V[79] and ωB97X-D3BJ[81] rank 5th–9th. DM21-D3BJ has the lowest systematic error (Figure 5, left) and is 2nd, 2nd, and 5th in the MAD, MAX, and RNG rankings, respectively. In particular, its MAD, MAX, and RNG are 0.273, 0.003, and 0.290 mh higher than the top-ranking DFA (the dispersion-uncorrected version of DM21 is within the top 15 DFAs only for MAX). The four Minnesota DFAs M08-HX,[74] M11,[75] M05-2X,[72] and M05-2X + D3[49,72] rank high. The best one is M05-2X, which ranks 3rd, 6th, and 3rd in the MAD, MAX, and RNG rankings, respectively. It is noteworthy that, in contrast to previous findings,[69] the ability of Minnesota DFAs to accurately calculate $\delta E_{45}^{\pm}$ is very slightly affected by dispersion correction. The high content of exact exchange in M05-2X, M08-HX, and M11 (56%, 52%, 43%, respectively) again witnesses the importance of the exchange interaction in TS energetics.

Both the analysis of the aggregate results and the data in Table 6 show that the conservative threshold of 0.1 mh is still beyond the energetic accuracy of currents DFAs, except for a few cases, for example, HN_3 + HC≡C–CN and HN_3 + H_2C=C–CHO.

A threshold of a few tenths of mh seems more feasible but in several cases a deviation of the order of or well beyond 1 mh is encountered. One cannot use even the best DFAs in a black-box manner to compute $\delta E_{45}^{\pm}$. With respect to $\delta E_{45}^{\pm} - \delta E_{45}^{\pm}$(W3X), we can recommend LC-BLYP, DM21-D3BJ, and ωB97M-D3BJ. The choice between these three DFAs should be guided by which measure (MAD, MAX, RNG) is most important in the problem at hand. If a compromise is sought for, DM21-D3BJ is probably the best choice. Our recommendation for $\delta E_{45}^{\pm} - \delta E_{45}^{\pm}$(W3X) of azide 1,3-DCs differ from previous, more general recommendations, which however assessed *barrier heights*. Indeed, investigations based on the updated BHPERI dataset[14] and the BH subset of GMTKN55[69] showed the superior accuracy of double-hybrids. Within our top 15 DFAs, M05-2X + D3 is the 3rd best hybrid DFA based on BHPERI, M08-HX + D3 and ωB97X–V are among the best three hybrids when assessed against the BH subset of GMTKN55,[69] and LC-ωPBE + D3BJ, CAM-B3LYP + D3BJ, and M11 were among the best five DFAs proposed for Diels–Alder reaction barrier height and regioselectivity when assessed against CCSD(T)/CBS data.[70]

Our discussion has so far considered the energetic difference between isomeric TSs, which best represents the ability of DFAs to mimic the high-level description provided by the W3X protocol. We can however adopt a more practical standpoint and consider the calculated yield of the 4-substituted product Y_4. Since

$$Y_4 - Y_4(\mathrm{W3X}) = \frac{1 - \exp\left[\frac{\delta E_{45}^{\pm} - \delta E_{45}^{\pm}(\mathrm{W3X})}{RT}\right]}{\left\{\exp\left[-\frac{\delta E_{45}^{\pm}(\mathrm{W3X})}{RT}\right] + \exp\left[\frac{\delta E_{45}^{\pm} - \delta E_{45}^{\pm}(\mathrm{W3X})}{RT}\right]\right\}\left\{1 + \exp\left[\frac{\delta E_{45}^{\pm}(\mathrm{W3X})}{RT}\right]\right\}} \quad (6)$$

the deviation of Y_4 from the reference depends on both $\delta E_{45}^{\pm} - \delta E_{45}^{\pm}(\mathrm{W3X})$ and $\delta E_{45}^{\pm}$ itself. So, this approach is less amenable to generalization, but it provides a more direct answer to our initial question. The difference $Y_4 - Y_4$(W3X) for all considered DFAs is summarized as bar charts in Figures 6 and S4. The number of DFAs including dispersion is 186. A threshold of $|Y_4 - Y_4(\mathrm{W3X})| \leq 0.5\%$ for all reactions selects the same equivalent DFAs as those previously selected using a 0.04 mh energetic threshold. Our set thus comprises 162 unique DFAs. The MSD is negative in most cases, mirroring the fact that in general DFAs excessively favor the 5-substituted product. The lowest systematic error is displayed by Minnesota DFAs (M11 has a remarkably low MSD = −0.038 mh), followed by the ωB97 and LC families, and DM21. Most of the best ranking DFAs are range-separated hybrids, which are followed by other hybrids and double hybrids. Double-hybrid DFAs are in the best half of the MSD ranking. The non-hybrid meta-GGA DFAs have the highest MSD. Dispersion is not critical to achieve low |MSD|.

Now consider MAD, MAX, and RNG (Figures 6 and S4). The bar charts show a similar shape. Starting from the lower end, the deviation decreases steadily and, in the case of MAD and RNG, finally there is a marked decrease for the best DFA, which again is LC-BLYP. Double-hybrid DFAs cluster towards large MAD and RNG, but are in the middle range for MAX. As to hybrid DFAs, GGA DFAs occupy most of the best half and meta-GGA hybrids are found throughout the deviation range but, in the case of MAD, the best ones cluster at the low MAD end.

Table 6. Deviation of the three recommended DFAs from the reference TS energy difference $\delta E_{45}^{\pm}$(W3X). All values are in mh.

	R	$\delta E_{45}^{\pm}$(W3X)	$\delta E_{45}^{\pm} - \delta E_{45}^{\pm}$(W3X) LC-BLYP	DM21-D3BJ	ωB97M-D3BJ
HC≡C–R	CHO	−0.885	−0.251	−1.121	−1.077
	CN	−0.432	0.010	−0.863	−0.873
	F	4.100	0.888	0.496	1.061
	Me	−0.405	0.462	0.402	0.359
	NH_2	−4.916	0.368	2.048	1.505
	OH	−2.257	0.682	0.005	1.246
H_2C=CH–R	CHO	−0.994	0.022	−1.364	−0.755
	CN	−2.928	0.122	−0.973	−0.870
	F	3.985	0.455	0.325	0.713
	Me	0.312	0.513	0.396	0.557
	NH_2	5.741	3.242	2.339	2.336
	OH	1.128	1.540	1.504	1.511

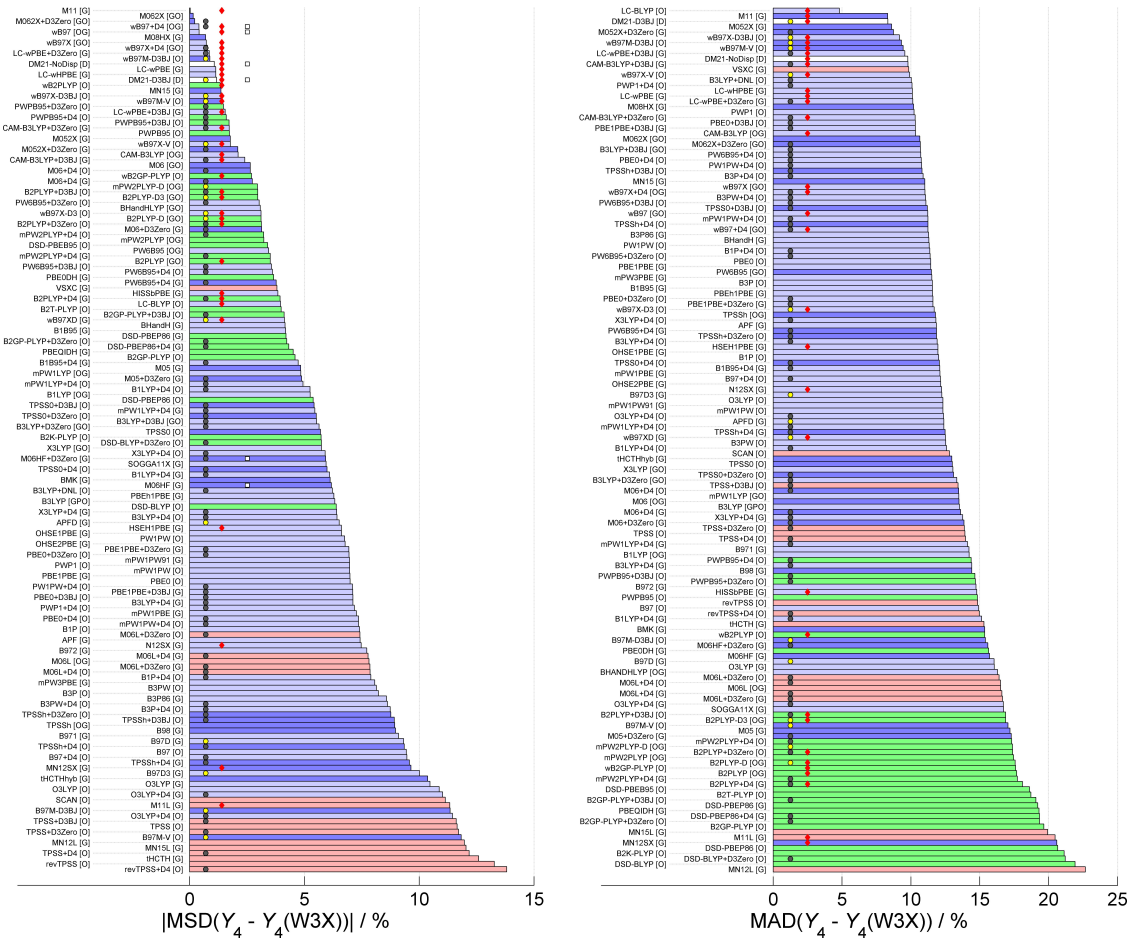

Figure 6. Mean signed (MSD) and mean absolute (MAD) difference Y_4-Y_4(W3X) calculated using all DFAs. The letter(s) in square brackets denote the software package. The absolute value of the MSD is plotted as most MSDs are negative. The white dots in the MSD bar chart indicate the six DFAs having positive MSD. Red: meta-GGA DFAs; light blue: hybrid GGA DFAs; dark blue; hybrid meta-GGA DFAs; green: double-hybrid DFAs; white: DM21. Additional information about the DFA type is given by symbols. Yellow dot: DFA including dispersion correction, gray dot: dispersion-corrected DFA. Red diamond: range-separated DFA.

Non-hybrid meta-GGA DFAs are scattered in the lower part of the bar charts with the notable exception of VSXC.[67] Range-separated DFAs are in general better than the global DFAs of the same type. Range-separated hybrid DFAs are required to have low Y_4-Y_4(W3X), with the exception of M05-2X and VSXC, again suggesting the importance of exchange and self-interaction error for the accurate description of forming bonds.[69]

We now focus on the 15 best DFAs for MAD, MAX, and RNG statistics (Table 7). In general, we observe less Minnesota DFAs and more DFAs of the ωB97 family. All statistics indicate that the investigated DFAs are not able to reproduce the reference Y_4 with an expected absolute deviation lower than 5%; deviations as large as ±20% can occur in specific cases. The three sets of the 15 top-ranking DFAs share 6 DFAs, 4 of which include dispersion correction (notably, the best DFA LC-BLYP is not dispersion corrected). This shows that they perform well in a robust way, i.e., independent of the considered statistics. The ranking, however, is very different. The 6 common DFAs are range-separated hybrids and DM21. Range-separated GGA hybrid LC-BLYP[71] has the lowest MAD, RNG, and MAX. It is particularly accurate on average (its MAD is about half of that of the second best DFA M11) and regarding the global variation range. However, LC-BLYP has MAX only marginally better than second-ranking ωB97X-D3BJ. M11 and DM21-D3BJ have good ranking in both MAD (2nd and 3rd, respectively) and MAX (5th and 3rd, respectively) but show large deviation on both sides of the reference Y_4. The ωB97M-D3BJ[79] and ωB97X-D3BJ[81] DFAs have good MAD and RNG ranking but they also have relatively poor RNG. In conclusion, with respect to Y_4-Y_4(W3X), LC-BLYP is clearly the best DFA.

In Table 8, detailed results for the LC-BLYP, M11, DM21-D3BJ, and ωB97X-D3BJ DFAs are collected. The largest deviations occur when Y_4(W3X) is close to 50%. In general, LC-BLYP has better accuracy, but it is not able to outperform the other DFAs in difficult cases (see HC≡C–Me and H_2C=CH–OH in Table 8). The isomeric yield accuracy for a given reaction depends on the DFA less strongly than the energetic accuracy $\delta E^{\pm}_{45}-\delta E^{\pm}_{45}$(W3X).

Both the analysis of the aggregate results and the data in Table 8 show that the desired general 1% accuracy in regioisomeric yield is still beyond the capability of currents

Table 7. The 15 top-ranking DFAs with respect to the MAD, MAX, and RNG statistics for the Y_4-Y_4(W3X) difference. The DFAs highlighted in bold occur in all three subsets.

MAD [%]		MAX [%]		RNG [%]	
10.1	PWP1 + D4	20.8	PW6B95 + D4	36.6	**M11**
10.0	B3LYP + DNL	20.7	LC-ωPBE	36.6	PW6B95 + D3BJ
9.9	ωB97X-V	20.7	LC-ωHPBE	**36.2**	**ωB97M-D3BJ**
9.8	VSXC	20.5	LC-ωPBE + D3BJ	**36.0**	**DM21-D3BJ**
9.8	**CAM-B3LYP + D3BJ**	20.3	ωB97X-V	**35.9**	**ωB97X-D3BJ**
9.8	DM21-NoDisp	20.3	PW6B95 + D3	35.8	PW6B95 + D4
9.6	LC-ωPBE + D3BJ	20.2	CAM-B3LYP	35.6	PW1PW + D4
9.4	ωB97M-V	19.6	**CAM-B3LYP + D3BJ**	35.2	PBE0 + D4
9.3	**ωB97M-D3BJ**	19.3	ωB97M-V	34.8	PWP1
9.2	**ωB97X-D3BJ**	19.0	CAM-B3LYP + D3	34.7	PWP1 + D4
8.7	M052X + D3	19.0	**M11**	34.6	**CAM-B3LYP + D3BJ**
8.6	M052X	18.7	**ωB97M-D3BJ**	34.5	TPSS0 + D3BJ
8.3	**DM21-D3BJ**	18.5	**DM21-D3BJ**	34.1	PBE1PBE + D3BJ
8.3	**M11**	18.5	**ωB97X-D3BJ**	34.1	PBE0 + D3BJ
4.8	**LC-BLYP**	17.6	**LC-BLYP**	22.7	**LC-BLYP**

Table 8. Deviation of the three recommended DFAs from the reference yield of the 4-substituted isomer Y_4(W3X) calculated for $T = 298$ K. All values are in %.

	R	Y_4(W3X)	Y_4-Y_4 (W3X) LC-BLYP	M11	DM21-D3BJ	ωB97X-D3BJ
HC≡C–R	CHO	72%	5%	17%	17%	17%
	CN	61%	0%	19%	19%	17%
	F	1%	−1%	−1%	−1%	−1%
	Me	61%	−12%	−5%	−10%	−9%
	NH_2	99%	−0%	−0%	−4%	−2%
	OH	92%	−7%	−17%	−0%	−18%
H_2C=CH–R	CHO	74%	0%	11%	18%	10%
	CN	96%	−1%	3%	3%	2%
	F	1%	−1%	−1%	−0%	−1%
	Me	42%	−12%	−8%	−10%	−14%
	NH_2	0%	0%	−0%	−0%	−0%
	OH	23%	−18%	−18%	−17%	−18%

DFAs. It is however achieved for 7 of the 12 investigated reactions. Of course, most of these have Y_4 close to 0% or 100%. A deviation of ±5% is expected, and a 20% error is not uncommon.

Conclusions

The presented set of calculations allowed us to understand that the calculation of the regioisomeric energy difference $\delta E_{45}^{\ddagger}$ and yield Y_4 of the 1,3-DC of HN_3 to simple monosubstituted alkynes and alkenes is not hopelessly difficult at the present state of theory, software, and hardware available to the computational chemist. Accurate regioselectivity requires that high-level benchmark calculations strive for the CBS limit of the CCSD(T) energy, accurately treat core-core/core-valence effects and include high-order excitations. Relativistic effects are of minor importance, at least for systems comprising atoms of the first two rows. DFT calculations are not able to provide an expected error of the TS energy difference better than ≈0.7 mh and errors ≈2 mh can occur in specific cases. Notwithstanding that both values are larger than the 0.1–0–2 threshold, the outlook is less pessimistic when the actual isomer yield is considered, since the best DFA LC-BLYP delivers an expected error of ±5%, though errors as large as 20% error are not rare. This can be compared with the ±5% accuracy of the conventional experimental determination of regioselectivity based on ^{1}H NMR spectroscopy, provided that nuclear relaxation times are correctly considered. More accurate treatment of exchange and self-interaction error is the key for improving the DFT results, whereas dispersion is of less importance. At present, an accuracy of 1–2% on the isomer yield is unfeasible but it seems that we are not far from achieving this goal, as far as electronic energy is concerned.

Although we tried to cover the chemical space of the azide 1,3-DC as completely as we could, one may wonder if our conclusions can be generalized. The main limitations of the current investigation are related to the calculation of benchmark $\delta E_{45}^{\ddagger}$ using high-level protocols and current mainstream hardware. The high computational and storage burden makes systems with more than 8 atoms of the 2nd row hardly feasible and prevents use of approaches to calculate rate constants more advanced than conventional TS theory (e.g., variational transition state approach[82]) The system size limitation precludes widening the scope of this type of investigation by considering larger substituents, which are common in synthetic work (such as aryls, for example, PhN_3, HC≡C–Ph) and including explicit solvent molecules (continuum solvent modeling is in

principle possible). It seems however possible to treat slightly larger azides (e.g., MeN_3) and/or dipolarophiles with other small substituents (e.g., $-CH_2X$, $-CH{=}X$, $-C{\equiv}X$, $-X-(CH_3)_n$, etc.) or two substituents (e.g., Me–C≡C–OH), or including 3rd row elements (e.g., P, SH, Cl). Treatment of the latter cases will improve (or disprove) the robustness of our conclusions and allow for better generalization of the 1,3-DC of azides to alkynes and alkenes. Further generalization to other 1,3-DCs will require analysis of cases with 1,3-dipoles other than azide.

Methods

We considered the TSs leading to the 4- and 5-substituted products of the uncatalyzed thermal 1,3-DC of the dipole HN_3 (as a model for organic azides) with the alkyne HC≡C–R and alkene $H_2C{=}CH{-}R$ (R=F, OH, NH_2, Me, CN, CHO) dipolarophiles. The choice of the substituent R was dictated by the conflicting demands of reasonable computational cost of high-level protocols and suitable coverage of the "reaction" space. A proper assessment of the DFAs for our chemical problem (regioisomerism) can be achieved if it is based on a set of reactions that represent as faithfully as possible the variety of dipolarophile substituents as perceived by both the computational chemist (electron demand, conjugation) and the synthetic chemist (synthetic scope). As "monoatomic" substituents we chose R=F, OH, NH_2, and Me, which cover largely different electronic demands and are typical of organic molecules, but neglected BH_2, BeH, and Li. To the former four substituents, we added CHO and CN since they are small, common organic substituents, which allow us to introduce conjugation between the dipolarophile reactive site and the substituent, thus enriching the investigated chemistry. The atom numbering and notation for the TSs are shown in Scheme 1.

Computational Methods

All calculations, both WF-based protocols and DFT, were carried out using the B3LYP/cc-pV(T+d)Z optimized TS structures in order to rank the methods purely regarding their ability to accurately compute the electronic energy difference $\delta E_{45}^{\pm} = E_4^{\pm} - E_5^{\pm}$. The TS nature of the optimized structures was checked calculating their vibrational frequencies in the RRHO approximation. The TAE[(T)] diagnostic[45] was calculated for all TSs using the aug'-cc-pVTZ basis set.

To compute benchmark $\delta E_{45}^{\pm}$ differences, we considered the following protocols: W1BD,[53] W1X-1,[54] W1-F12,[13] W2X,[55] W2-F12,[13] WMS,[56] and W3X.[57] W4-type protocols[45] are too computationally expensive, especially regarding storage, for mainstream hardware. W1BD is based on a Brueckner doubles calculation improved with perturbative triples and including core-core/core-valence (CC/CV) and Douglas–Kroll–Hess (DKH) second-order scalar relativistic contributions. All other protocols use HF/CABS as a reference to calculate the CCSD(T) energy using different basis sets (including the explicitly correlated set for the F12 approach) and extrapolation schemes; they also include CC/CV and DKH contributions calculated using MP2 or CCSD with different basis sets and extrapolation schemes. The W3X protocol is W1X-1 augmented with energy contributions from coupled-cluster non-perturbative triple [T−(T)] and perturbative quadruple (Q) excitations.

The B3LYP TS optimizations and W1BD calculations were carried out using Gaussian 16/A.03.[59] All other WF-based protocols were carried out using Molpro 2010.1-80[83] and MRCC.2019-02-09,[84] in most cases using the scripts generously provided by the authors. Basis sets were obtained from the Basis Set Exchange site.[85]

We calculated $\delta E_{45}^{\pm}$ using meta-GGA, hybrid, and double hybrid DFAs that are pre-defined in Gaussian 16/A.03[59] and ORCA 4.2.1.[60,61] We used Jensen's pcseg family[62] of basis sets since they were optimized for DFT calculations. For DFAs not including dispersion correction, $\delta E_{45}^{\pm}$ was also calculated using dispersion correction based on the D3,[49,50] D3BJ,,[50,51] D4[52] and VV10[64] methods, whenever the appropriate parameterization is available.

For ORCA 4.2.1 we checked that the isomeric energy difference is saturated with respect to the basis set cardinality, integration grid, integral accuracy, and SCF threshold by calculating the energy of the two TSs for the $HN_3 + HC{\equiv}CF$ reaction with the ωB97X[86] and M06-2X[73] DFAs (the latter is known to be sensitive to the grid choice[16]). Using the pcseg-3 quadruple-zeta basis set in conjunction with options Grid6 (Lebedev 590 integration grid), IntAcc=7 (determines no. of grid radial points) and TightSCF (energy threshold $=10^{-8}$ hartree), we commit an error in $\delta E_{45}^{\pm} < 0.01$ mh. With these choices, the rotational invariance (i.e., the dependence on the molecular orientation with respect to the cartesian axes) of $\delta E_{45}^{\pm}$ of the $HN_3 + HC{\equiv}CF$ 1,3-DC calculated using M06-2X is about 0.01 mh. For Gaussian 16/A.03 we used options as close as possible to those selected for ORCA, i.e., SCF(Conver=8) and Int(Grid=75590), in order to have comparable results.

Since several DFAs are implemented in both Gaussian16 and ORCA, we compared the isomeric $E_i^{\pm}$ and $\delta E_{ij}^{\pm}$ calculated using B3LYP,[87] O3LYP,[88,89] M06-2X, and ωB97X (Table 9). While the two program suites give very close values for B3LYP, M06-2X, and ωB97X, differences are significantly larger (and substituent dependent) for O3LYP. There can be multiple reasons for these discrepancies, including different implementations of the DFAs. Therefore, in the following analysis, we separately considered nominally identical DFAs in Gaussian16 and ORCA. The results obtained were then pairwise compared to assess the significance of possible differences.

Finally, we considered the recent neural-network-trained DFA DeepMind 21 (DM21).[63] The latter, which can be described as a local range-separated hybrid DFA, was reported to perform very well at the calculation of the reaction barriers present in the GMTKN55 database.[34] DM21 calculations were carried out using Python 3.9.5, NumPy 1.19.5, SciPy 1.7.1, and PySCF 2.0.1.

Most calculations were carried out on a Linux cluster comprising 10 nodes with 16–20 Intel Xeon E5-2407 CPUs and 64 GB RAM; the most demanding CCSDT and CCSDT(Q) calculations were carried out on single nodes with E5620 CPUs and 144 GB RAM.

Table 9. Comparison of the isomeric TS energy difference $\delta E_{45}^{\pm}$ computed by Gaussian16 A.03 and ORCA 4.2.1 for selected DFAs. The mean signed difference (MSD) and mean absolute difference/MAD) over the 12 1,3-DC reactions are given along with the maximum and minimum differences.

Method	MSD [μh]	MAD [μh]	max [μh]	min [μh]
B3LYP	−6.9	6.9	7.0	−21.1
O3LYP	114.8	323.9	635.7	−1339.9
M06-2X	−1.9	3.5	9.3	−13.8
ωB97X	−0.9	5.6	16.1	−14.1

Methods to Compare Results to Reference

To assess the ability of a given method, we have to compare the distance of its results from the reference results. The simplest deviation measure is the energetic difference $\delta E_{45}^{\ddagger} - \delta E_{45}^{\ddagger}$(reference). In the present case, we chose the highest-level protocol W3X as a reference method. When assessing DFAs, we deemed not necessary to subtract the Rel contribution from $\delta E_{45}^{\ddagger}$(W3X) before comparing the latter to $\delta E_{45}^{\ddagger}$(DFA) as the Rel correction is so small (<0.07 mh) not to affect the comparison.

Using $\delta E_{45}^{\ddagger} - \delta E_{45}^{\ddagger}$(W3X) neglects the fact that $\delta E_{45}^{\ddagger}$ spans more than an order of magnitude. A given energetic difference has unequal importance when it occurs for reactions with $\delta E_{45}^{\ddagger}$ much larger or smaller than *RT* since the sensitivity of isomer yield Y_i to $\delta E_{45}^{\ddagger}$ is highest when $\delta E_{45}^{\ddagger} \ll RT$. So, for more practical considerations, we also calculated the $Y_4 - Y_4$(W3X) deviation of the product yield.

As statistical indices for $\delta E_{45}^{\ddagger} - \delta E_{45}^{\ddagger}$(W3X) and $Y_4 - Y_4$(W3X), we computed the mean absolute deviation (MAD), the maximum absolute deviation (MAX), the range of signed deviations (RNG), and the mean signed deviation (MSD) over the 12 considered 1,3-DCs. While MSD indicates a "systematic" deviation from the reference values, MAD, MAX, and RNG allow one to estimate the average, maximum, and spread of the deviation from the W3X reference.

Acknowledgements

Open Access funding provided by Consiglio Nazionale delle Ricerche within the CRUI-CARE Agreement.

Conflict of Interest

The authors declare no conflict of interest.

Data Availability Statement

The data that support the findings of this study are available from the corresponding author upon reasonable request.

Keywords: 1,3-dipolar cycloaddition · azides · benchmark, DFT · regioselectivity

[1] K. V. Gothelf, K. A. Jørgensen, *Chem. Rev.* **1998**, *98*, 863–910.
[2] J. I. Seeman, *Chem. Rec.* **2022**, *22*, e202100212.
[3] R. B. Woodward, R. Hoffmann, *Angew. Chem. Int. Ed. Engl.* **1969**, *8*, 781–853.
[4] K. Fukui, *Acc. Chem. Res.* **1971**, *4*, 57–64.
[5] K. Fukui, *Angew. Chem. Int. Ed. Engl.* **1982**, *21*, 801–809.
[6] K. N. Houk, Joyner. Sims, R. E. Duke, R. W. Strozier, J. K. George, *J. Am. Chem. Soc.* **1973**, *95*, 7287–7301.
[7] K. N. Houk, Joyner. Sims, C. R. Watts, L. J. Luskus, *J. Am. Chem. Soc.* **1973**, *95*, 7301–7315.
[8] G. Molteni, A. Ponti, *Chem. Eur. J.* **2003**, *9*, 2770–2774.
[9] J. A. Montgomery, M. J. Frisch, J. W. Ochterski, G. A. Petersson, *J. Chem. Phys.* **1999**, *110*, 2822–2827.
[10] D. H. Ess, K. N. Houk, *J. Am. Chem. Soc.* **2008**, *130*, 10187–10198.
[11] G. O. Jones, K. N. Houk, *J. Org. Chem.* **2008**, *73*, 1333–1342.
[12] F. S. Vilhena, F. M. Bickelhaupt, J. W. M. Carneiro, *Eur. J. Org. Chem.* **2017**, *2017*, 4313–4318.
[13] A. Karton, J. M. L. Martin, *J. Chem. Phys.* **2012**, *136*, 124114.
[14] A. Karton, L. Goerigk, *J. Comput. Chem.* **2015**, *36*, 622–632.
[15] W. Koch, M. C. Holthausen, *A Chemist's Guide to Density Functional Theory*, Wiley-VCH, Weinheim, **2001**.
[16] N. Mardirossian, M. Head-Gordon, *Mol. Phys.* **2017**, *115*, 2315–2372.
[17] D. H. Ess, G. O. Jones, K. N. Houk, *Adv. Synth. Catal.* **2006**, *348*, 2337–2361.
[18] P. Geerlings, F. De Proft, W. Langenaeker, *Chem. Rev.* **2003**, *103*, 1793–1874.
[19] R. K. Roy, S. Krishnamurti, P. Geerlings, S. Pal, *J. Phys. Chem. A* **1998**, *102*, 3746–3755.
[20] F. Méndez, J. Tamariz, P. Geerlings, *J. Phys. Chem. A* **1998**, *102*, 6292–6296.
[21] A. Ponti, *J. Phys. Chem. A* **2000**, *104*, 8843–8846.
[22] A. K. Chandra, M. Tho Nguyen, *J. Comput. Chem.* **1998**, *19*, 195–202.
[23] A. K. Chandra, T. Uchimaru, M. T. Nguyen, *J. Chem. Soc. Perkin Trans. 2* **1999**, 2117–2121.
[24] L. T. Nguyen, F. D. Proft, V. L. Dao, M. T. Nguyen, P. Geerlings, *J. Phys. Org. Chem.* **2003**, *16*, 615–625.
[25] G. Molteni, A. Ponti, *Molecules* **2021**, *26*, 928.
[26] L. Domingo, *Molecules* **2016**, *21*, 1319.
[27] S. Zeghada, G. Bentabed-Ababsa, A. Derdour, S. Abdelmounim, L. R. Domingo, J. A. Sáez, T. Roisnel, E. Nassar, F. Mongin, *Org. Biomol. Chem.* **2011**, *9*, 4295.
[28] H. B. El Ayouchia, B. Lahoucine, H. Anane, M. Ríos-Gutiérrez, L. R. Domingo, S.-E. Stiriba, *ChemistrySelect* **2018**, *3*, 1215–1223.
[29] S. A. Lopez, M. E. Munk, K. N. Houk, *J. Org. Chem.* **2013**, *78*, 1576–1582.
[30] F. Schoenebeck, D. H. Ess, G. O. Jones, K. N. Houk, *J. Am. Chem. Soc.* **2009**, *131*, 8121–8133.
[31] D. H. Ess, G. O. Jones, K. N. Houk, *Org. Lett.* **2008**, *10*, 1633–1636.
[32] A. Zeroual, *OAJTMR* **2017**, *1*, 1–4.
[33] S. Yu, P. Vermeeren, K. Dommelen, F. M. Bickelhaupt, T. A. Hamlin, *Chem. Eur. J.* **2020**, *26*, 11529–11539.
[34] L. Goerigk, S. Grimme, *J. Chem. Theory Comput.* **2010**, *6*, 107–126.
[35] A. Karton, *J. Phys. Chem. A* **2019**, *123*, 6720–6732.
[36] H. C. Kolb, M. G. Finn, K. B. Sharpless, *Angew. Chem. Int. Ed. Engl.* **2001**, *40*, 2004–2021.
[37] C. W. Tornøe, C. Christensen, M. Meldal, *J. Org. Chem.* **2002**, *67*, 3057–3064.
[38] J. R. Johansson, T. Beke-Somfai, A. Said Stålsmeden, N. Kann, *Chem. Rev.* **2016**, *116*, 14726–14768.
[39] W. G. Kim, M. E. Kang, J. B. Lee, M. H. Jeon, S. Lee, J. Lee, B. Choi, P. M. S. D. Cal, S. Kang, J.-M. Kee, G. J. L. Bernardes, J.-U. Rohde, W. Choe, S. Y. Hong, *J. Am. Chem. Soc.* **2017**, *139*, 12121–12124.
[40] W. Song, N. Zheng, *Org. Lett.* **2017**, *19*, 6200–6203.
[41] S. Kumar, S. L. Khokra, A. Yadav, *Futur. J. Pharm. Sci.* **2021**, *7*, 106.
[42] B. I. Taggert, C. Walker, D. Chen, U. Wille, *Sci. Rep.* **2021**, *11*, 14980.
[43] A. Karton, *WIREs Comput. Mol. Sci.* **2016**, *6*, 292–310.
[44] L. Goerigk, N. Mehta, *Aust. J. Chem.* **2019**, *72*, 563.
[45] A. Karton, E. Rabinovich, J. M. L. Martin, B. Ruscic, *J. Chem. Phys.* **2006**, *125*, 144108.
[46] A. Tajti, P. G. Szalay, A. G. Császár, M. Kállay, J. Gauss, E. F. Valeev, B. A. Flowers, J. Vázquez, J. F. Stanton, *J. Chem. Phys.* **2004**, *121*, 11599–11613.
[47] T. Helgaker, P. Jørgensen, J. Olsen, *Molecular Electronic-Structure Theory*, Wiley, Chichester, New York, USA, **2000**.
[48] L. Goerigk, S. Grimme, *WIREs Comput. Mol. Sci.* **2014**, *4*, 576–600.
[49] S. Grimme, J. Antony, S. Ehrlich, H. Krieg, *J. Chem. Phys.* **2010**, *132*, 154104.
[50] D. G. A. Smith, L. A. Burns, K. Patkowski, C. D. Sherrill, *J. Phys. Chem. Lett.* **2016**, *7*, 2197–2203.
[51] S. Grimme, S. Ehrlich, L. Goerigk, *J. Comput. Chem.* **2011**, *32*, 1456–1465.
[52] E. Caldeweyher, S. Ehlert, A. Hansen, H. Neugebauer, S. Spicher, C. Bannwarth, S. Grimme, *J. Chem. Phys.* **2019**, *150*, 154122.
[53] E. C. Barnes, G. A. Petersson, J. A. Montgomery, M. J. Frisch, J. M. L. Martin, *J. Chem. Theory Comput.* **2009**, *5*, 2687–2693.
[54] B. Chan, L. Radom, *J. Chem. Theory Comput.* **2012**, *8*, 4259–4269.
[55] B. Chan, L. Radom, *J. Chem. Theory Comput.* **2015**, *11*, 2109–2119.
[56] Y. Zhao, L. Xia, X. Liao, Q. He, M. X. Zhao, D. G. Truhlar, *Phys. Chem. Chem. Phys.* **2018**, *20*, 27375–27384.
[57] B. Chan, L. Radom, *J. Chem. Theory Comput.* **2013**, *9*, 4769–4778.
[58] N. C. Handy, J. A. Pople, M. Head-Gordon, K. Raghavachari, G. W. Trucks, *Chem. Phys. Lett.* **1989**, *164*, 185–192.

[59] M. J. Frisch, G. W. Trucks, H. B. Schlegel, G. E. Scuseria, M. A. Robb, J. R. Cheeseman, G. Scalmani, V. Barone, G. A. Petersson, H. Nakatsuji, X. Li, M. Caricato, A. V. Marenich, J. Bloino, B. G. Janesko, R. Gomperts, B. Mennucci, H. P. Hratchian, J. V. Ortiz, A. F. Izmaylov, J. L. Sonnenberg, D. Williams-Young, F. Ding, F. Lipparini, F. Egidi, J. Goings, B. Peng, A. Petrone, T. Henderson, D. Ranasinghe, V. G. Zakrzewski, J. Gao, N. Rega, G. Zheng, W. Liang, M. Hada, M. Ehara, K. Toyota, R. Fukuda, J. Hasegawa, M. Ishida, T. Nakajima, Y. Honda, O. Kitao, H. Nakai, T. Vreven, K. Throssell, J. A. Montgomery Jr., J. E. Peralta, F. Ogliaro, M. J. Bearpark, J. J. Heyd, E. N. Brothers, K. N. Kudin, V. N. Staroverov, T. A. Keith, R. Kobayashi, J. Normand, K. Raghavachari, A. P. Rendell, J. C. Burant, S. S. Iyengar, J. Tomasi, M. Cossi, J. M. Millam, M. Klene, C. Adamo, R. Cammi, J. W. Ochterski, R. L. Martin, K. Morokuma, O. Farkas, J. B. Foresman, D. J. Fox, Gaussian 16, revision A.03, Gaussian, Inc., Wallingford CT (USA), **2016**.
[60] F. Neese, *WIREs Comput. Mol. Sci.* **2012**, *2*, 73–78.
[61] F. Neese, *WIREs Comput. Mol. Sci.* **2018**, *8*, e1327, DOI 10.1002/wcms.1327.
[62] F. Jensen, *J. Chem. Theory Comput.* **2014**, *10*, 1074–1085.
[63] J. Kirkpatrick, B. McMorrow, D. H. P. Turban, A. L. Gaunt, J. S. Spencer, A. G. D. G. Matthews, A. Obika, L. Thiry, M. Fortunato, D. Pfau, L. R. Castellanos, S. Petersen, A. W. R. Nelson, P. Kohli, P. Mori-Sánchez, D. Hassabis, A. J. Cohen, *Science* **2021**, *374*, 1385–1389.
[64] O. A. Vydrov, T. Van Voorhis, *J. Chem. Phys.* **2010**, *133*, 244103.
[65] Y. Zhao, D. G. Truhlar, *J. Phys. Chem. A* **2006**, *110*, 13126–13130.
[66] N. Mehta, J. M. L. Martin, *J. Chem. Theory Comput.* **2022**, *18*, 5978–5991.
[67] T. Van Voorhis, G. E. Scuseria, *J. Chem. Phys.* **1998**, *109*, 400–410.
[68] J. Sun, A. Ruzsinszky, J. P. Perdew, *Phys. Rev. Lett.* **2015**, *115*, 036402.
[69] L. Goerigk, A. Hansen, C. Bauer, S. Ehrlich, A. Najibi, S. Grimme, *Phys. Chem. Chem. Phys.* **2017**, *19*, 32184–32215.
[70] D. Loco, I. Chataigner, J. Piquemal, R. Spezia, *ChemPhysChem* **2022**, *23*, DOI 10.1002/cphc.202200349.
[71] Y. Tawada, T. Tsuneda, S. Yanagisawa, T. Yanai, K. Hirao, *J. Chem. Phys.* **2004**, *120*, 8425–8433.
[72] Y. Zhao, N. E. Schultz, D. G. Truhlar, *J. Chem. Theory Comput.* **2006**, *2*, 364–382.
[73] Y. Zhao, D. G. Truhlar, *Theor. Chem. Acc.* **2008**, *120*, 215–241.
[74] Y. Zhao, D. G. Truhlar, *J. Chem. Theory Comput.* **2008**, *4*, 1849–1868.
[75] R. Peverati, D. G. Truhlar, *J. Phys. Chem. Lett.* **2011**, *2*, 2810–2817.
[76] T. M. Henderson, A. F. Izmaylov, G. Scalmani, G. E. Scuseria, *J. Chem. Phys.* **2009**, *131*, 044108.
[77] O. A. Vydrov, G. E. Scuseria, *J. Chem. Phys.* **2006**, *125*, 234109.
[78] T. Yanai, D. P. Tew, N. C. Handy, *Chem. Phys. Lett.* **2004**, *393*, 51–57.
[79] N. Mardirossian, M. Head-Gordon, *J. Chem. Phys.* **2016**, *144*, 214110.
[80] A. Najibi, L. Goerigk, *J. Chem. Theory Comput.* **2018**, *14*, 5725–5738.
[81] J.-D. Chai, M. Head-Gordon, *Phys. Chem. Chem. Phys.* **2008**, *10*, 6615–6620.
[82] J. L. Bao, D. G. Truhlar, *Chem. Soc. Rev.* **2017**, *46*, 7548–7596.
[83] H.-J. Werner, P. J. Knowles, G. Knizia, F. R. Manby, M. Schütz, *WIREs Comput. Mol. Sci.* **2012**, *2*, 242–253.
[84] M. Kállay, P. R. Nagy, D. Mester, L. Gyevi-Nagy, J. Csóka, B. Szabó, Z. Rolik, G. Samu, J. Csontos, B. Hégely, Á. Ganyecz, I. Ladjánszki, L. Szegedy, B. Ladóczki, K. Petrov, M. Farkas, P. D. Mezei, R. A. Horváth, MRCC, a quantum chemical program suite, Budapest University of Technology and Economics, Budapest (Hungary), **2019**.
[85] B. P. Pritchard, D. Altarawy, B. Didier, T. D. Gibson, T. L. Windus, *J. Chem. Inf. Model.* **2019**, *59*, 4814–4820.
[86] J.-D. Chai, M. Head-Gordon, *J. Chem. Phys.* **2008**, *128*, 084106.
[87] P. J. Stephens, F. J. Devlin, C. F. Chabalowski, M. J. Frisch, *J. Phys. Chem.* **1994**, *98*, 11623–11627.
[88] W.-M. Hoe, A. J. Cohen, N. C. Handy, *Chem. Phys. Lett.* **2001**, *341*, 319–328.
[89] A. J. Cohen, N. C. Handy, *Mol. Phys.* **2001**, *99*, 607–615.

Manuscript received: February 16, 2023
Revised manuscript received: March 7, 2023
Accepted manuscript online: March 10, 2023
Version of record online: ■■, ■■

RESEARCH ARTICLE

The regioselectivity of the uncatalyzed cycloaddition between HN_3 and 12 dipolarophiles (HC≡C–R and H_2C=CH–R), calculated using a large set of density functional approximations, was compared to benchmark values obtained by the W3X protocol. The best density functional approximation LC-BLYP delivers a ±5% average error, but 10–20% errors are also present.

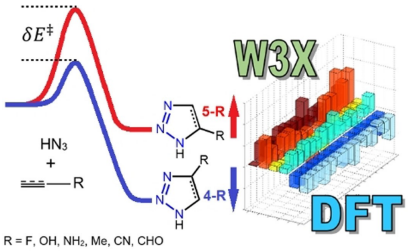

*Dr. G. Molteni, Dr. A. Ponti**